Area waves on a slender vortex revisited

Stephen Childress & Andrew D. Gilbert

Mathematics Department,
College of Engineering, Mathematics and Physical Sciences,
University of Exeter, EX4 4QF, U.K.

Abstract

This paper considers the classic problem of the dynamics of axisymmetric waves on a rectilinear vortex, in the absence of viscosity. The waves alter the axial pressure distribution and thus generate axial flows which depend on the radial distribution of vorticity. To simplify this problem, models have been introduced which average over the cross-section and eliminate the radial dependence. One approach, pioneered by Lundgren & Ashurst (1989), *J. Fluid Mech.* **200**, 283–307, averages the momentum equation. Another averaging method, due to Leonard (1994), *Phys. Fluids* **6**, 765–777, focuses on the vorticity equation. The present paper takes a fresh look at the derivation of these two distinct models, which we refer to as the *momentum wave model* and *vorticity wave model* respectively, using the tools of differential geometry to develop a hybrid Eulerian–Lagrangian approach. We compare these models with area waves in the asymptotic limit of a slender vortex, with radial structure retained. Numerical calculations are presented to show the differences between waves in the full slender vortex system and those in the momentum and vorticity wave models. We also discuss modification of the vorticity wave model to allow an external irrotational flow, and simulations are presented where a vortex is subjected to uniform axial stretching. Our approach can also be developed to model more complicated configurations, such as occur during vortex collisions.

Key words: vortex stretching, area waves, Euler equation, Lagrangian coordinates, vortex collision

1 Introduction

The study of waves and instabilities on vortices has a long history in fluid mechanics, as reviewed for example in Saffman (1992). The present paper concerns the classic topic of waves on a vortex in axisymmetric geometry, for inviscid, incompressible flow. The basic mechanism behind these *area waves* is straightforward (Lundgren & Ashurst, 1989; Abid *et al.*, 2002). Suppose we have an axisymmetric vortex column dependent only on radius r in cylindrical polar coordinates (r, θ, z). Axial vorticity ω_3 corresponds to azimuthal velocity $v \equiv u_2$, in the θ direction. If the radius of the cross section is reduced at some axial location z, conservation

of angular momentum will cause the vortex to spin faster there, lowering the pressure at the vortex centre. The low pressure will drive an axial flow that tends to increase the vortex radius at z. This restoring mechanism drives standing waves on a vortex column, made up as the sum of two propagating waves moving on a fast time-scale, the wave velocity being related to the vortex turnover time. We can also explain this process using vorticity (Leonard, 1994): if we squeeze a vortex and so increase the azimuthal velocity locally, the variation in this velocity component along the axis will lead to the winding up of axial vorticity ω_3 to generate azimuthal vorticity ω_2: uncurling this component using the right hand rule confirms that this corresponds to an axial flow towards the squeezed region. From either perspective, the axial fluid flow is coupled to variations in the radius or area along a vortex, hence the term area waves (Lundgren & Ashurst, 1989).

Looking to a more general geometry, several authors have considered the dynamics of vortex filaments, the axial vorticity being localized near a curve $\mathcal{C}(t)$ in $\mathbb{R}^3$. Incorporating an additional axial flow corresponds to including an azimuthal component of vorticity, one that circulates around $\mathcal{C}$. The equations for vortex dynamics in this limit were first elaborated in papers by Ting and co-workers (Tung & Ting, 1967; Ting, 1971; Callegari & Ting, 1978), reviewed in the book Ting, Klein & Knio (2007). In these papers the effect of axial flow is incorporated in multiple-scale expansions of the Navier–Stokes equations, the short scale being the vortex width and the large scale being the typical radius of curvature of $\mathcal{C}$. These are matched to give equations for the internal evolution of the vortex and for its motion, valid both with and without viscosity. In these works, the time-scale used is that of the motion of the filaments, and the vorticity and flows are taken to be independent of the fast area wave / vortex turnover time-scale. This then factors out area waves, and means that the leading order flow or vorticity components must satisfy certain compatibility conditions. At a similar time, Widnall, Bliss & Zalay (1971) and Widnall & Bliss (1971) investigated the effects of axial flow on the motion of vortex rings and perturbed filaments, and Moore & Saffman (1972) developed equations for inviscid vortex motion using a force balance method, equating the forces on each side of the boundary of the vortex filament. The resulting equations were also derived in Fukumoto & Miyazaki (1991), by working from the vorticity equation and applying systematic expansions to the Biot–Savart law. In the studies of Moore & Saffman (1972) and Fukumoto & Miyazaki (1991), the effects of axial flow on the overall vortex motion are identified, but the fast internal dynamics of the axial flow are removed from the system by assuming a uniform core radius, $a = a(t)$ only at leading order. The large scale motion of vortex filaments occurs on a slower time scale than the vortex turnover time, and the solvability condition that ensures there is no evolution on the fast area wave time scale — in other words no area waves — is just that the radius a depends only on time and not on the axial coordinate.

There have also been a number of studies allowing area waves. Lundgren & Ashurst (1989) and Marshall (1991, 1993) derive equations based on momentum balance, while Klein & Majda (1991a,b), Leonard (1994), Margerit & Brancher (2001) and Margerit (2002) work from the vorticity equation; see Ting, Klein & Knio (2007) for a review of these and further papers. One goal of these papers is to develop simplified equations for area waves, where the properties of the vortex depend only upon the axial coordinate and time. Such models involve some sort of averaging over the radial coordinate and result in hyperbolic systems of equations, leading to area waves which steepen into shocks. Other studies and numerical simulations confirm the many phenomena that can occur on the scale of a vortex core. From their numerical simulations,

Melander & Hussain (1994) stress that the core dynamics shows neither pure mass transport nor pure wave motion, and that the results are sensitive to the Reynolds number. Many of the studies cited above consider the further issue of vortex breakdown, reviewed in Leibovich (1978).

Our paper builds on the two seminal studies of Lundgren & Ashurst (1989), henceforth referred to as LA89, and Leonard (1994), henceforth referred to as L94. In LA89, an equation given below by (2.18) in Eulerian coordinates (z, t) describes area waves on a columnar vortex. Here $A(z, t)$ gives the area occupied by the vorticity in the filament at axial location z and time t, and $W(z, t)$ is the corresponding axial flow. Conservation of mass gives the equation (2.10) and the coupled nonlinear equations may be solved numerically. The LA89 model is based on conservation of momentum and so the resulting equation has a conservation form for the axial velocity W. Although our focus is on purely axisymmetric vortex geometry, we should note that LA89 considers the more general geometry of an arbitrary vortex filament, building on the study of Moore & Saffman (1972).

In the second study, of L94, the same problem is addressed starting from the vorticity equation and by averaging terms over the cross section, leads to an equation of the form (2.26) below. [1] Although the resulting equation is very similar to (2.18), with the replacement of the material transport term $D_t W$ by $A\, D_t(W/A)$, the physics is different, in that W/A is proportional to the azimuthal vorticity ω_2 in the system. This is the natural quantity that is transported from the perspective of vortex dynamics (as discussed further in section 2). To give a simple picture: if a vortex with a mean axial flow W is stretched out along its length using a pure strain field, by a factor K, then the axial vorticity $\omega_3 \to K\omega_3$, the azimuthal vorticity $\omega_2 \to K^{-1/2}\omega_2$ and the corresponding axial flow $w \to K^{-1}w$. Since the area $A \to K^{-1}A$, it is W/A that is conserved rather than W. We refer to equation (2.26) of L94 here as the *vorticity wave model*, as its physics are very different from what we will call the *momentum wave model* (2.18) of LA89. We stress that both models involve a radial averaging of the full dynamics that is not a rational approximation in a mathematical sense: something has to give when we reduce the (r, z, t) dependence to simply (z, t) dependence in the PDEs. For this reason we refer to each of these using the term *model* below. Both models for area waves are derived in an Eulerian framework in §2 below.

Our first goal in the present paper is to develop an analytical and numerical understanding of area waves, and compare the above two heuristic models with the exact system for waves on a columnar vortex. For this comparison we make use of the slender vortex or long wavelength limit. As in the paper L94, we are particularly interested in following the evolution of vorticity. Consequently, our focus will be on the Lagrangian description of a fluid flow, which is superior to the Eulerian description for tracking the advection and stretching of vorticity. As we explain and qualify below, the coordinate system we use is adapted to the shape of the vortex, and equations are derived that allow the coordinates to evolve in time, following area waves on a vortex column. For numerical simulations, Eulerian or Lagrangian approaches could be deployed, but again for tracking vorticity a Lagrangian approach has many advantages: the vorticity distribution is essentially fixed and it is the mapping into physical space that is evolved.

[1] Some of the constants in (2.26) differ from L94 because of the choice of weighting in the cross sectional average, as we discuss later.

Our second goal is to begin to develop the analytical tools to study vortex dynamics with axial flow in more complicated geometries than that of axisymmetric area waves on a columnar vortex. We would like to have at our disposal tools to follow vortex dynamics in complex three-dimensional situations including vortex stretching and collisions, incorporating also axial flow. From this perspective what is paramount is to follow and appropriately conserve the vorticity distribution during advection and stretching using a Lagrangian framework, an Eulerian framework being insufficient to do this. This is a longer term ambition, to revisit and extend what is a complicated and well-studied classical problem of general vortex motion (see Saffman, 1992; Ting, Klein & Knio, 2007, and references therein). Towards this ambition, we here focus on waves on a rectilinear axisymmetric vortex, as both an important problem in its own right and as a test bed for the development of methods for modelling vortices with axial flow in more complex situations.

The remainder of the paper is structured as follows: in section 3 we start with an exact formulation of the equations of motion and the vorticity equation in axisymmetric geometry. Our approach is novel in that we use Lagrangian coordinates, or more strictly *hybrid Eulerian–Lagrangian coordinates* (Soward & Roberts, 2010) as discussed in detail below. Here, our Lagrangian coordinates track vorticity surfaces as the vortex flexes in response to area wave motions. The approach allows us to write down exact equations for the vortex in a form which builds in the conservation of vorticity. The point is that the Lagrangian map is responsible for mapping what is essentially a fixed axial vorticity distribution onto a more general vortex in physical space. Although our focus is on time-dependent phenomena, in the case of a steady flow the coordinates we use correspond to von Mises coordinates, applied to vortex dynamics with axial flow by Klein & Ting (1992). To set up our Lagrangian framework, we first adopt methods from differential geometry to write down the equations in a very general coordinate system in §3.1. This section involves machinery that may be unfamiliar to some readers, and can be skipped, as we set out the full governing equations in coordinate form in §3.2. We then discuss the choices made to allow the coordinate system to follow the axisymmetric vortex geometry in §4. We take the mathematical limit of a slender vortex in §5, and numerical simulations in §5.3 will exhibit area waves, the formation of shocks (at which point the slender vortex system is no longer valid), and the development of internal structure.

In section 6, we derive the vorticity wave model in a Lagrangian frame, by averaging the vorticity equation over radius to remove radial dependence. As in §2, we need to make assumptions that are heuristic, in that they do not arise from a rational approximation to the equations taken in an appropriate limit. Instead an average of the axial flow is taken at a key point of the development to close the system. Our approach and the resulting equations are broadly similar to those in L94, whose analysis is based on taking moments of the vorticity equation, although we remark that L94 additionally includes effects of shorter wavelengths, which are missing in our model. We then present numerical simulations comparing the two model systems — the momentum wave model of LA89 and the vorticity wave model of L94 — with the full slender vortex dynamics.

One advantage of a vorticity formulation is that an external irrotational flow, for example time-dependent axial stretching (Marshall, 1992; Nolan, 2001; Abid *et al.*, 2002) is easily incorporated into the governing equations. In our Lagrangian framework an external flow only modifies the boundary conditions used for inverting the elliptic problem for the velocity, and

so it is easily incorporated into the slender body system or the vorticity wave model. In anticipation of future applications of these methods to problems involving vortex interactions and collisions, we introduce imposed axisymmetric external flows to both the full slender body system and to the vorticity wave model. In §7 we study the effects of a uniform external strain field and find that the area waves tend to become frozen as the restoring effect is weakened, leading to the emergence of a passively stretched area profile at long times. We consider external irrotational flows that depend on space and time in §8, with a focus on those having a similarity form, and give concluding discussion in §9.

2 Momentum and vorticity wave models from an Eulerian perspective

All of our models are based on the approximation of a slender vortex tube, so we begin with a summary of the slender vortex limit. We shall then derive the momentum wave model of LA89 and vorticity wave model of L94 from an Eulerian perspective.

In this section coordinates are the usual cylindrical polars (r, θ, z) and vector components are referred to the usual unit vectors $(\hat{\boldsymbol{r}}, \hat{\boldsymbol{\theta}}, \hat{\boldsymbol{z}})$. We consider a slender vortex, that is the limit when the vortex length and axial scale ℓ satisfies $\ell \gg 1$, as compared with the vortex radius $a(z,t)$ which is taken to be of order unity. This then fixes an appropriate time scale and yields the scalings

$$\partial_t, \partial_z = O(\ell^{-1}), \quad \partial_r = O(1), \quad \partial_\theta = 0, \quad u = O(\ell^{-1}), \quad v, w = O(1), \quad p = O(1). \tag{2.1}$$

The leading order governing equations for the velocity $\boldsymbol{u} = (u, v, w)$ are

$$-r^{-1}v^2 + p_r = 0, \tag{2.2}$$
$$\partial_t(rv) + u(rv)_r + w(rv)_z = 0, \tag{2.3}$$
$$\partial_t w + uw_r + ww_z + p_z = 0, \tag{2.4}$$
$$r^{-1}(ru)_r + w_z = 0. \tag{2.5}$$

The only simplification of this approximation is in the radial momentum balance, allowing a direct calculation of pressure as a radial integral of $r^{-1}v^2$. The corresponding vorticity $\boldsymbol{\omega}$ has components $(\omega_1, \omega_2, \omega_3)$, and of these we need only

$$\omega_2 = -w_r, \quad \omega_3 = r^{-1}\partial_r(rv), \tag{2.6}$$

since ω_1 is of order ℓ^{-2}. Note that the axial vorticity ω_3 is here given exactly whereas the formula for the azimuthal vorticity ω_2 neglects a term $\partial u/\partial z$, meaning that in regions where ω_2 is zero, there is also no axial flow at leading order (unless it is r-independent and so imposed externally). From (2.2, 2.4) the quantity $\chi = \omega_2/r$ obeys the equation

$$\partial_t\chi + u\chi_r + w\chi_z = \partial_z(v^2/r^2). \tag{2.7}$$

We now turn to the simpler models of interest to us. We take the vortex boundary to be a circle at each z station

$$r = a(z,t), \tag{2.8}$$

with all vorticity confined to $r \le a$. The cross sectional area $A(z,t)$ and mean flow $W(z,t)$ are defined by

$$A(z,t) = \pi a^2, \quad W(z,t) = \langle w \rangle \equiv A^{-1} \int_0^a w(r,z,t)\, 2\pi r\, dr. \tag{2.9}$$

It is then a consequence of conservation of volume (2.5) that

$$\partial_t A + \partial_z (AW) = 0. \tag{2.10}$$

We now neeed to choose a vortex structure with which to do calculations. The most straightforward course is to take axial vorticity ω_3 to be independent of radius for $r \le a(z,t)$. Given such a Rankine vortex has constant circulation Γ along its length, this choice gives the uniform (as a function of r) profile

$$\omega_3(z,t) = \Gamma / A(z,t), \quad r \le a, \tag{2.11}$$

and zero outside, that is for $r > a$. The corresponding azimuthal velocity v is given by (2.6),

$$v = \begin{cases} \Gamma r / 2A, & r \le a, \\ \Gamma / 2\pi r, & r > a, \end{cases} \tag{2.12}$$

and integrating to infinity, the pressure field from (2.2) is

$$p = \begin{cases} p_\infty - \Gamma^2/4\pi A + \Gamma^2 r^2 / 8A^2, & r \le a, \\ p_\infty - \Gamma^2 / 8\pi^2 r^2, & r > a. \end{cases} \tag{2.13}$$

This gives the basic vortex structure.

To obtain the LA89 equation we focus on the axial momentum equation (2.4) and take the axial flow as a uniform 'slug flow' profile

$$w(r,z,t) = W(z,t), \quad r \le a, \tag{2.14}$$

and zero outside. This cannot truly be correct since radial dependence arises from the pressure field (2.13). So instead of satisfying (2.4) at each point (r,z), we integrate this equation over a fixed volume V given by $z_1 \le z \le z_2$ and $0 \le r \le R$ where R is larger than $a(z,t)$ for all (z,t), and z_1, z_2 are arbitrary. Note that $w = 0$ on $r = R$. Making use of (2.13, 2.14), for the individual terms we obtain:

$$\int_V \partial_t w \, dV = \partial_t \int_V w \, dV = \partial_t \int_{z_1}^{z_2} AW \, dz = \int_{z_1}^{z_2} \partial_t (AW)\, dz, \tag{2.15}$$

$$\begin{aligned} \int_V (u w_r + w w_z)\, dV &= \int_V \boldsymbol{u} \cdot \nabla w \, dV = \int_V \nabla \cdot (\boldsymbol{u} w)\, dV = \int_{\partial V} \boldsymbol{u} w \cdot \boldsymbol{n} \, dS \\ &= \left[\int_0^a w^2 \, 2\pi r \, dr \right]_{z_1}^{z_2} = \left[AW^2 \right]_{z_1}^{z_2} = \int_{z_1}^{z_2} \partial_z (AW^2)\, dz, \end{aligned} \tag{2.16}$$

$$\int_V p_z \, dV = \int_{z_1}^{z_2} \int_0^R p_z \, 2\pi r \, dr \, dz = \int_{z_1}^{z_2} \frac{\Gamma^2 A_z}{4\pi A^3} \int_0^a (A - \pi r^2)\, 2\pi r \, dr \, dz = \int_{z_1}^{z_2} \frac{\Gamma^2 A_z}{8\pi A} \, dz. \tag{2.17}$$

Putting these together and making use of (2.10) gives

$$D_t W \equiv (\partial_t + W \partial_z) W = \frac{\Gamma^2}{8\pi} \, \partial_z \left(\frac{1}{A} \right), \tag{2.18}$$

which is the LA89 momentum wave model in Eulerian coordinates.

The alternative approach of L94 applies a similar process to the azimuthal vorticity equation in the form (2.7). Inside the vortex $r \le a$, the right-hand side $\partial_z(v^2/r^2)$ is independent of r from (2.12), so this suggests taking χ independent of r. We thus set

$$\omega_2 = r\chi(z,t), \quad r \le a, \tag{2.19}$$

and zero outside. Integrating (2.6) gives the axial flow inside as

$$w = \tfrac{1}{2}\chi(a^2 - r^2), \quad r \le a. \tag{2.20}$$

It may then be checked that the mean flow $W = \chi A/4\pi$ and so we can write

$$w = 2W(1 - \pi r^2/A), \quad \omega_2 = 4\pi r W/A, \quad r \le a. \tag{2.21}$$

Again this quadratic axial velocity profile will not provide a solution of the full problem — the vorticity equation (2.7) will not be satisfied pointwise — and so we apply (2.7) integrated over the volume V defined above. The various terms are

$$\int_V \partial_t\chi \, dV = \partial_t \int_V \chi \, dV = \partial_t \int_V 4\pi W/A \, dV = \partial_t \int_{z_1}^{z_2} 4\pi W \, dz = \int_{z_1}^{z_2} 4\pi \, \partial_t W \, dz, \tag{2.22}$$

$$\begin{aligned}\int_V (u\chi_r + w\chi_z)\, dV &= \int_V \boldsymbol{u}\cdot\nabla\chi \, dV = \int_V \nabla\cdot(\boldsymbol{u}\chi)\, dV = \int_{\partial V} \boldsymbol{u}\chi\cdot\boldsymbol{n}\, dS \\ &= \Big[\int_0^a w\chi \, 2\pi r \, dr\Big]_{z_1}^{z_2} = \big[4\pi W^2\big]_{z_1}^{z_2} = \int_{z_1}^{z_2} 4\pi\, \partial_z W^2 \, dz,\end{aligned} \tag{2.23}$$

$$\int_V \partial_z(v^2/r^2)\, dV = \int_{z_1}^{z_2}\int_0^a -\tfrac{1}{2}\Gamma^2 A^{-3}\, \partial_z A \, 2\pi r \, dr \, dz = \int_{z_1}^{z_2} -\tfrac{1}{2}\Gamma^2 A^{-2}\, \partial_z A \, dz. \tag{2.24}$$

Putting this together yields

$$\partial_t W + \partial_z W^2 = \frac{\Gamma^2}{8\pi}\, \partial_z \left(\frac{1}{A}\right). \tag{2.25}$$

We can rewrite this to bring in the material derivative $D_t = \partial_t + W\partial_z$, using (2.10), in the form

$$AD_t\left(\frac{W}{A}\right) = A(\partial_t + W\partial_z)\left(\frac{W}{A}\right) = \frac{\Gamma^2}{8\pi}\, \partial_z \left(\frac{1}{A}\right). \tag{2.26}$$

Although this equation, governing what we call the vorticity wave model of L94, involves W, it is best viewed as an equation governing azimuthal vorticity $\omega_2 = r\chi \propto rW/A$ in (2.21).

That W/A is the relevant quantity in the transport equation (2.26) for vorticity may also be seen by considering how vorticity behaves under a strain field. While for area waves the local strain is generated by variations along the vortex, the most tractable example is a uniform rectilinear vortex (independent of z) subjected to an externally imposed uniform strain field. We therefore briefly consider the flow field $\boldsymbol{u}$ and vorticity field $\boldsymbol{\omega}$ of the form

$$\boldsymbol{u} = -\tfrac{1}{2}\kappa(t) r\hat{\boldsymbol{r}} + v(r,t)\hat{\boldsymbol{\theta}} + [\kappa(t)z + W(r,t)]\hat{\boldsymbol{z}}, \tag{2.27}$$

$$\boldsymbol{\omega} = \omega_2(r,t)\hat{\boldsymbol{\theta}} + \omega_3(r,t)\hat{\boldsymbol{z}}, \tag{2.28}$$

with $\omega_2 = -\partial_r W$, $\omega_3 = r^{-1}\partial_r(rv)$. The function $\kappa(t)$ gives the time-dependence of the external irrotational strain field (and in later notation we will write the external axial flow component as $W_{\rm ext} = \kappa(t)z$). The vorticity equation then gives

$$\partial_t\omega_2 - \tfrac{1}{2}\kappa r\,\partial_r\omega_2 = -\tfrac{1}{2}\kappa\omega_2, \quad \partial_t\omega_3 - \tfrac{1}{2}\kappa r\,\partial_r\omega_3 = \kappa\omega_3. \tag{2.29}$$

With the use of the Lagrangian radial variable s given by

$$s = re^{-\frac{1}{2}K(t)}, \quad K(t) = \int_0^t \kappa(\tau)\,d\tau, \tag{2.30}$$

the solution is

$$\omega_2 = e^{-\frac{1}{2}K(t)}\,\omega_{20}(s), \quad \omega_3 = e^{K(t)}\,\omega_{30}(s), \quad v = e^{\frac{1}{2}K(t)}\,v_0(s), \quad W = e^{-K(t)}\,W_0(s), \tag{2.31}$$

the subscript zero denoting initial conditions. It is evident that what is conserved is W/A, since areas shrink as $A \propto e^{-K(t)}$. If the stretching amplitude $\kappa(t)$ is non-zero just for a finite time interval, then the vorticity and velocity distributions before and after are simply related through the quantity K from an integration over that time window. While W/A is conserved, the momentum W in the axial flow is changed during the time interval by the pressure forces linked to the externally imposed irrotational flow. In fact examination of the Euler equation shows that the pressure field is

$$p = (\tfrac{1}{4}\partial_t\kappa - \tfrac{1}{8}\kappa^2)r^2 - \tfrac{1}{2}(\partial_t\kappa + \kappa^2)z^2 - \int_r^\infty \rho^{-1}V^2(\rho)\,d\rho, \tag{2.32}$$

up to the addition of a constant and so there are both r- and z-dependent terms that appear in the axial momentum equation in the presence of an external strain field.

As we have already noted, both the momentum wave model (2.18) and the vorticity wave model (2.26) involve a judicious, but in some ways arbitrary, averaging of the governing equations, and so the approximations are heuristic rather than rational in the strict mathematical sense. If our interest is in the vorticity dynamics of filaments, with an eye to vortex stretching and vortex collisions, the second of these has the proper vorticity conservation properties, even in the presence of stretching. In short, in the second model the main approximation is in the advecting flow field rather than in the vorticity distribution. Note that (2.26) is not quite the same as that derived in L94, where weighted moments of the vorticity equation are taken rather than the average over the vortex cross section as here. For example to calculate the average axial transport of ω_2 in L94, the axial flow is weighted by the strength of ω_2. The effect of this is to give an equation of the same structure, but with different constants. A choice of weighting could be used to fine-tune any model based on LA89 or L94, but in the present paper we will just use a straightforward average.

It is worth noting that the two models, (2.18) and (2.26), really are distinct, having different dispersion relations. We linearise (2.10) and for the momentum wave model (2.18), about $W = W_0$, $A = A_0$ to obtain

$$\omega/k - W_0 = \pm\Gamma/\sqrt{8\pi A_0}, \tag{2.33}$$

for disturbances proportional to $e^{ikz-i\omega t}$. This gives disturbances travelling at the same velocity upstream or downstream relative to the uniform axial flow W_0. However for the vorticity wave

model (2.26) the dispersion relation is

$$\omega/k - W_0 = \tfrac{1}{2}W_0 \pm \tfrac{1}{2}\sqrt{W_0^2 + \Gamma^2/2\pi A_0}. \tag{2.34}$$

Thus for small W_0 we regain (2.33), while for large W_0

$$\omega/k - W_0 \simeq W_0 \quad \text{or} \quad -\Gamma^2/2\pi A_0 W_0, \tag{2.35}$$

and waves propagate more rapidly downstream than upstream (L94). We will test this against the full slender body system in sections 5 and 6.

3 Governing equations

We turn now to a derivation of the equations for slender axisymmetric vortex dynamics using a coordinate system that is adapted to the geometry of vortex lines: in particular our aim is to simplify the description of the nested surfaces on which vortex lines spiral. As these surfaces are axisymmetric our coordinate system will be chosen to simplify the axial and radial components of vorticity (rather than the azimuthal component). We consider a vortex in *physical space* $\tilde{\mathcal{M}} = \mathbb{R}^3$ with cylindrical polar coordinates $(\tilde{r}, \tilde{\theta}, \tilde{z})$ as depicted in figure 1(a). The vortex is axisymmetric, independent of the coordinate $\tilde{\theta}$, with boundary $\tilde{r} = \tilde{a}(\tilde{z}, \tilde{t})$. We have now made a major change of notation from the previous section by adorning quantities in physical space with tildes. We will use untilded variables for quantities referred to the moving coordinate system, to be defined shortly. We find it convenient to use bold letters for vector fields, differential forms or other tensors. We use light typeface for coordinates, scalar fields and tensor components.

We adopt a new (r, θ, z) coordinate system, in which vortex lines lie on surfaces given by $r =$ const. and varying $\theta = \tilde{\theta}$ and z. This can be viewed as in figure 1 as a map ϕ from cylindrical vortex surfaces in (r, θ, z) coordinates in panel (b), to time-dependent curved vortex surfaces in physical space, panel (a). We wish to write down the equations of motion in the physical space $\tilde{\mathcal{M}}$ with respect to the (r, θ, z) coordinate system; however these coordinates are curvilinear, non-orthogonal, and unsteady. In addition to the choice of coordinates, we need to adopt bases for the various vector fields employed. To do this in a systematic fashion we need the language of classical differential geometry. In the next section we will set out the theory in coordinate-free form. Readers who are unfamiliar with this approach can skip section 3.1 and move directly to section 3.2, which gives the results in explicit coordinate form.

3.1 Fluid flow in a geometric setting

We now make a change of gear, and in this section only we discuss the equations for fluid motion in an entirely abstract setting. We assume some standard background in differential geometry, including vector fields, differential forms, the Lie derivative $\mathcal{L}$, the inner product $\lrcorner$, the musical raising and lowering operators $\sharp$ and $\flat$, and the exterior derivative d; see for example, Hawking & Ellis (1973), Schutz (1980), Frankel (1997), Besse & Frisch (2017) or

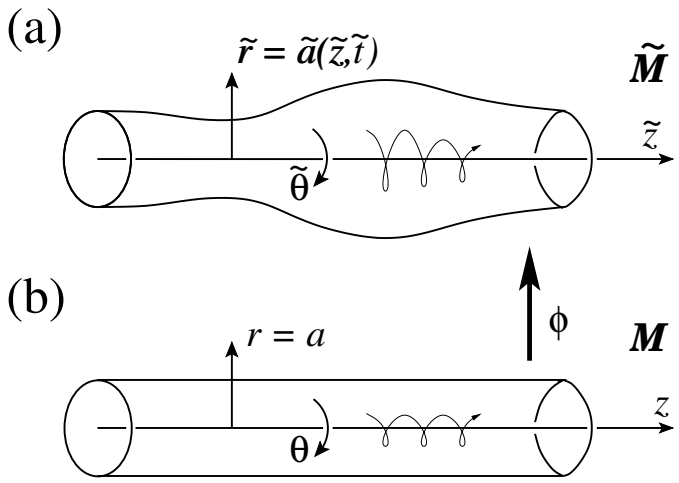

Fig. 1. Vortex (a) shown in physical space $\tilde{\mathcal{M}}$ with cylindrical polar coordinates $(\tilde{r}, \theta, \tilde{z})$, and (b) represented in the space $\mathcal{M}$ with coordinates (r, θ, z). A map ϕ takes points in $\mathcal{M}$ to points in $\tilde{\mathcal{M}}$ and a single vortex line is depicted in both geometries.

Webb (2018). We also write various key formulae in components in appendix A, as this may be more familiar to some readers.

Although our vortex always lies in ordinary Euclidean space $\mathbb{R}^3$ and is axisymmetric, we set out the equations for incompressible, inviscid fluid dynamics in a general form valid for any three-dimensional orientable manifold $\tilde{\mathcal{M}}$ equipped with a metric $\tilde{\boldsymbol{g}}$ and induced volume form $\tilde{\boldsymbol{\mu}}$. The fluid flow is given by a time-dependent velocity field $\tilde{\boldsymbol{u}}(\tilde{\boldsymbol{x}}, \tilde{t})$ defined at points $\tilde{\boldsymbol{x}}$ in $\tilde{\mathcal{M}}$ and times $\tilde{t}$. It will be divergence free, so that $d(\tilde{\boldsymbol{u}} \lrcorner \tilde{\boldsymbol{\mu}}) = 0$. The corresponding *momentum* $\tilde{\boldsymbol{\nu}}$ of the fluid is defined to be the 1-form field given by applying the metric to the velocity field, with $\tilde{\boldsymbol{\nu}} = \tilde{\boldsymbol{g}}(\tilde{\boldsymbol{u}}, \cdot) = \tilde{\boldsymbol{u}}_{\tilde{\flat}}$. A standard argument based on the variational principle for classical mechanics (see, e.g., Arnold & Khesin, 1998) gives the equations governing ideal, incompressible fluid motion as

$$\partial_{\tilde{t}}\, \tilde{\boldsymbol{\nu}} + \mathcal{L}_{\tilde{\boldsymbol{u}}}\, \tilde{\boldsymbol{\nu}} + d(\tilde{p} - \tfrac{1}{2} \tilde{\boldsymbol{u}} \lrcorner \tilde{\boldsymbol{\nu}}) = 0, \tag{3.1}$$

$$\tilde{\boldsymbol{\nu}} = \tilde{\boldsymbol{u}}_{\tilde{\flat}} = \tilde{g}(\tilde{\boldsymbol{u}}, \cdot), \tag{3.2}$$

$$d(\tilde{\boldsymbol{u}} \lrcorner \tilde{\boldsymbol{\mu}}) = 0. \tag{3.3}$$

Here $\tilde{p}$ is the usual pressure field, and the Lie derivative term $\mathcal{L}_{\tilde{\boldsymbol{u}}}\, \tilde{\boldsymbol{\nu}}$ expresses transport of momentum in the flow field. Since $\lrcorner$ denotes a contraction or inner product, we can write $\tilde{\boldsymbol{u}} \lrcorner \tilde{\boldsymbol{\nu}} = g(\tilde{\boldsymbol{u}}, \tilde{\boldsymbol{u}}) = |\tilde{\boldsymbol{u}}|^2$. We can also apply the exterior derivative d to obtain an equation for the vorticity $\tilde{\boldsymbol{\zeta}} = d\tilde{\boldsymbol{\nu}}$,

$$\partial_{\tilde{t}}\, \tilde{\boldsymbol{\zeta}} + \mathcal{L}_{\tilde{\boldsymbol{u}}}\, \tilde{\boldsymbol{\zeta}} = 0, \tag{3.4}$$

$$\tilde{\boldsymbol{\zeta}} = d\tilde{\boldsymbol{\nu}}, \tag{3.5}$$

with of course $d\tilde{\boldsymbol{\zeta}} = d^2 \tilde{\boldsymbol{\nu}} = 0$.

We wish now to use moving coordinates for the vortex in the physical space $\tilde{\mathcal{M}} = \mathbb{R}^3$, as depicted in figure 1(a). We will define moving coordinates (r, θ, z) with $\theta = \tilde{\theta}$ and (r, z) adapted to follow the axisymmetric surfaces on which vortex lines (generally spirals) lie. We can think of our vortex as sitting in another space $\mathcal{M} = \mathbb{R}^3$ with coordinates (r, θ, z), where

it has a simpler structure. A time-dependent map ϕ then takes points from $\mathcal{M}$ to $\tilde{\mathcal{M}}$. This is depicted in figure 1(b): in $\mathcal{M}$ the vortex lines lie on cylindrical surfaces of constant r for $r \leq a$ where a is the (now constant) radius of the vortex. In $\mathcal{M}$ the flow is also much simplified, as we discuss below. Much of the dynamics of the vortex in the physical space $\tilde{\mathcal{M}}$ is now hidden inside the map ϕ.

Our next goal is to write down the equations for the fluid flow using the coordinate system (r, θ, z) based in $\mathcal{M}$. We first proceed formally, in full generality. Suppose that $(\tilde{x}^1, \tilde{x}^2, \tilde{x}^3)$ are *any* (fixed) coordinates on $\tilde{\mathcal{M}}$ (these need not be Cartesian nor orthogonal), and suppose we have a time-dependent map ϕ from points labelled by (fixed) coordinates (x^1, x^2, x^3) on a manifold $\mathcal{M}$, to points on $\tilde{\mathcal{M}}$,

$$(\tilde{x}^1, \tilde{x}^2, \tilde{x}^3) = \phi(x^1, x^2, x^3, t). \tag{3.6}$$

We will use both $\tilde{t}$ and t as time variables, with $t = \tilde{t}$. Now, if we fix a coordinate point (x^1, x^2, x^3) in $\mathcal{M}$, the image point under ϕ traces a path in $\tilde{\mathcal{M}}$ as time t varies, and this specifies a (generally time-dependent) vector field $\tilde{\boldsymbol{U}}$ on $\tilde{\mathcal{M}}$: this is the velocity of the moving coordinate system on $\tilde{\mathcal{M}}$, formally

$$\tilde{\boldsymbol{U}} = \partial_t \phi \circ \phi^{-1}. \tag{3.7}$$

We assume that ϕ is a diffeomorphism at all times t, and is as smooth as is needed in subsequent manipulations. We can then apply a *pull back* ϕ^* by the map ϕ to the above equations (3.1–3.5) to obtain

$$\partial_t \boldsymbol{\nu} + \mathcal{L}_{\boldsymbol{u}-\boldsymbol{U}} \boldsymbol{\nu} + d(p - \tfrac{1}{2}\boldsymbol{u} \lrcorner \boldsymbol{\nu}) = 0, \tag{3.8}$$
$$\partial_t \boldsymbol{\zeta} + \mathcal{L}_{\boldsymbol{u}-\boldsymbol{U}} \boldsymbol{\zeta} = 0, \tag{3.9}$$

now regrouped, with

$$\boldsymbol{\nu} = \boldsymbol{u}_\flat = \boldsymbol{g}(\boldsymbol{u}, \cdot), \tag{3.10}$$
$$d(\boldsymbol{u} \lrcorner \boldsymbol{\mu}) = 0, \tag{3.11}$$
$$\boldsymbol{\zeta} = d\boldsymbol{\nu}. \tag{3.12}$$

Here we have denoted the pulled back fields by removing the tilde label, so that for example,

$$\boldsymbol{u} = \phi^* \tilde{\boldsymbol{u}}, \quad \boldsymbol{\nu} = \phi^* \tilde{\boldsymbol{\nu}}, \quad \boldsymbol{U} = \phi^* \tilde{\boldsymbol{U}}, \quad \boldsymbol{g} = \phi^* \tilde{\boldsymbol{g}}, \quad p = \phi^* \tilde{p}. \tag{3.13}$$

Equations (3.8–3.12) hold because pull backs commute with the exterior derivative d, the Lie derivative $\mathcal{L}$ and contraction, and because the following identity holds for any tensor field $\boldsymbol{\tau}$:

$$\phi^* \, \partial_{\tilde{t}} \, \tilde{\boldsymbol{\tau}} = \partial_t \, \boldsymbol{\tau} - \mathcal{L}_{\boldsymbol{U}} \, \boldsymbol{\tau}. \tag{3.14}$$

In this identity the first time derivative, denoted $\partial_{\tilde{t}}$, is taken at a point on $\tilde{\mathcal{M}}$ with coordinates $(\tilde{x}^1, \tilde{x}^2, \tilde{x}^3)$ fixed, while the second time derivative ∂_t, with $t = \tilde{t}$, is taken with the coordinates (x^1, x^2, x^3) held fixed, that is a fixed point on $\mathcal{M}$ but a moving point on $\tilde{\mathcal{M}}$. This is a straightforward generalisation to any tensor object of the usual identity '$\partial_t = D_t - \boldsymbol{U} \cdot \nabla$' used for the material derivative 'D_t' in fluid dynamics.

We will work with the system of equations (3.8–3.12), but it is convenient to rewrite these by defining $\boldsymbol{u} = \boldsymbol{U} + \boldsymbol{v}$ so that, while $\boldsymbol{u}$ is the full velocity field, $\boldsymbol{v}$ is the velocity relative to

the moving coordinate system. We can also use Cartan's formula

$$\mathcal{L}_{\boldsymbol{v}}\,\boldsymbol{\alpha} = d(\boldsymbol{v}\lrcorner\boldsymbol{\alpha}) + \boldsymbol{v}\lrcorner d\boldsymbol{\alpha}, \tag{3.15}$$

valid for any differential form $\boldsymbol{\alpha}$.[2] The dynamical equations are rewritten most conveniently as

$$\partial_t\,\boldsymbol{\nu} + \boldsymbol{v}\lrcorner d\boldsymbol{\nu} + d\pi = 0, \tag{3.16}$$
$$\partial_t\,\boldsymbol{\zeta} + d(\boldsymbol{v}\lrcorner\boldsymbol{\zeta}) = 0, \tag{3.17}$$

with

$$\pi = p + \tfrac{1}{2}\boldsymbol{v}\lrcorner\boldsymbol{\nu} - \tfrac{1}{2}\boldsymbol{U}\lrcorner\boldsymbol{\nu}, \tag{3.18}$$
$$\boldsymbol{u} = \boldsymbol{U} + \boldsymbol{v}. \tag{3.19}$$

The full set of governing equations is then (3.16–3.19) together with (3.10–3.12): note that we have written down equations for both momentum and vorticity for completeness but will focus on the latter in what follows.

We remark that if the coordinate system is entirely Lagrangian, then we have $\boldsymbol{u} = \boldsymbol{U}$ and $\boldsymbol{v} = 0$; the map ϕ is then the Lagrangian map of fluid parcels from their initial positions to those at a general time t. In this case the vorticity is constant with respect to the moving coordinate system, $\partial_t\boldsymbol{\zeta} = 0$, so that vorticity in $\mathcal{M}$ is given by the field values at time $t = 0$, $\boldsymbol{\zeta} = \boldsymbol{\zeta}_0$. In physical space $\tilde{\mathcal{M}}$, vorticity $\tilde{\boldsymbol{\zeta}}$ is then given by the push forward in the flow map from the initial condition, $\tilde{\boldsymbol{\zeta}} = \phi_*\,\boldsymbol{\zeta}_0$; this is the Cauchy solution as discussed by Besse & Frisch (2017).

However there is no need to use an entirely Lagrangian coordinate system: we can choose to absorb into the flow $\boldsymbol{U}$ whatever component of the motion we wish, dealing then with the residue $\boldsymbol{v}$. There is considerable freedom here, and the acid test is whether it simplifies the problem at hand. This approach is sometimes referred to as *hybrid Euler–Lagrange* (e.g., Soward & Roberts, 2010); in the present context we can think of the coordinate system as taking care of part of the motion of Lagrangian parcels, with velocity $\boldsymbol{U}$, while the remaining $\boldsymbol{v}$ is the Eulerian residue. For example this method is at the heart of Generalised Lagrangian Mean (GLM) and related theories, where $\boldsymbol{U}$ gives a mean flow, and the $\boldsymbol{v}$ component tracks waves or other fluctuations; see Bühler (2014), Gilbert & Vanneste (2018), and references therein.

It is worth noting that there is a compatibility condition between the flow $\boldsymbol{U}$ of the coordinate system and the metric $\boldsymbol{g}$. In the physical space $\tilde{\mathcal{M}}$ the metric $\tilde{\boldsymbol{g}}$ is steady, in other words $\partial_{\tilde{t}}\,\tilde{\boldsymbol{g}} = 0$. Looking at (3.14) it then follows that in $\mathcal{M}$, the pulled back metric $\boldsymbol{g}$ is generally time-dependent and satisfies

$$\partial_t\,\boldsymbol{g} - \mathcal{L}_{\boldsymbol{U}}\,\boldsymbol{g} = 0. \tag{3.20}$$

Alternatively this can be seen as an equation that evolves the metric $\boldsymbol{g}$ given the flow $\boldsymbol{U}$. It can be verified that the velocity field $\boldsymbol{U}$ and metric $\boldsymbol{g}$ used below satisfy this condition; we omit the details.

[2] Note that this formula gives the commonly used identities of vector calculus for $\boldsymbol{a}\times(\nabla\times\boldsymbol{b})$ and $\nabla\times(\boldsymbol{a}\times\boldsymbol{b})$; see for example Webb (2018).

We now set out the equations in full component form. In preparation for future calculations we will move to cylindrical polar coordinate labels $(x^1, x^2, x^3) \to (r, \theta, z)$, but we stress that the coordinates are entirely arbitrary at this point; there is no assumption of axisymmetry, for example.

The Euler equation, at a fundamental level, governs the transport of momentum $\boldsymbol{\nu}$ in a fluid flow with velocity field $\boldsymbol{u}$. Although these are usually identified in Euclidean space with Cartesian coordinates, here the components ν_i and u^i are linked by the metric $\boldsymbol{g}$ for the coordinate system:

$$\nu_i = g_{ij}\, u^j. \tag{3.21}$$

In fact these components are referred to the standard coordinate bases, so that for example

$$\boldsymbol{u} = u^1 \partial_r + u^2 \partial_\theta + u^3 \partial_z, \quad \boldsymbol{\nu} = \nu_1\, dr + \nu_2\, d\theta + \nu_3\, dz \tag{3.22}$$

(in traditional language u^i are simply the contravariant components of velocity and ν_i the covariant components). The fluid flow is incompressible, which may be expressed in coordinate form as

$$\partial_i(\mu u^i) = 0. \tag{3.23}$$

Here $|\boldsymbol{g}| = \mu^2$ is the determinant of the metric tensor, so that

$$\boldsymbol{\mu} = \mu\, dr \wedge d\theta \wedge dz \tag{3.24}$$

is the standard volume form, with $\mu > 0$.

Now our coordinate system is itself time-dependent, and at any point in physical space a fixed coordinate point moves with velocity $\boldsymbol{U}$. Thus we define the velocity $\boldsymbol{v}$ relative to the coordinate system by $\boldsymbol{u} = \boldsymbol{U} + \boldsymbol{v}$, or

$$u^i = U^i + v^i. \tag{3.25}$$

The Euler equation (3.16, 3.18) then transports momentum relative to the moving coordinate system via

$$(\partial_t + v^1\partial_r + v^2\partial_\theta + v^3\partial_z)\nu_1 - v^1\nu_{1r} - v^2\nu_{2r} - v^3\nu_{3r} + \pi_r = 0, \tag{3.26}$$
$$(\partial_t + v^1\partial_r + v^2\partial_\theta + v^3\partial_z)\nu_2 - v^1\nu_{1\theta} - v^2\nu_{2\theta} - v^3\nu_{3\theta} + \pi_\theta = 0, \tag{3.27}$$
$$(\partial_t + v^1\partial_r + v^2\partial_\theta + v^3\partial_z)\nu_3 - v^1\nu_{1z} - v^2\nu_{2z} - v^3\nu_{3z} + \pi_z = 0, \tag{3.28}$$
$$\pi = p + \tfrac{1}{2}(v^1\nu_1 + v^2\nu_2 + v^3\nu_3 - U^1\nu_1 - U^2\nu_2 - U^3\nu_3), \tag{3.29}$$

using here letter subscripts or ∂ for derivatives, and numerical ones for components. Although there are numerous terms here, many cancel out or are zero in typical applications once a metric is put in and the relations (3.21) and (3.25) are applied.

For the vorticity equation it is convenient to define components ζ_i by

$$\boldsymbol{\zeta} = \zeta_1\, d\theta \wedge dz + \zeta_2\, dz \wedge dr + \zeta_3\, dr \wedge d\theta, \tag{3.30}$$

with, from (3.12),

$$\zeta_1 = \nu_{3\theta} - \nu_{2z}, \quad \zeta_2 = \nu_{1z} - \nu_{3r}, \quad \zeta_3 = \nu_{2r} - \nu_{1\theta}, \tag{3.31}$$

which satisfy

$$\zeta_{1r} + \zeta_{2\theta} + \zeta_{3z} = 0 \tag{3.32}$$

(this is just $d\boldsymbol{\zeta} = 0$). The vorticity equation (3.17) can then be written in a variety of ways, of which we prefer

$$(\partial_t + v^1\partial_r + v^2\partial_\theta + v^3\partial_z)\zeta_1 - (\zeta_1\partial_r + \zeta_2\partial_\theta + \zeta_3\partial_z)v^1 + (v^1_r + v^2_\theta + v^3_z)\zeta_1 = 0, \tag{3.33}$$
$$(\partial_t + v^1\partial_r + v^2\partial_\theta + v^3\partial_z)\zeta_2 - (\zeta_1\partial_r + \zeta_2\partial_\theta + \zeta_3\partial_z)v^2 + (v^1_r + v^2_\theta + v^3_z)\zeta_2 = 0, \tag{3.34}$$
$$(\partial_t + v^1\partial_r + v^2\partial_\theta + v^3\partial_z)\zeta_3 - (\zeta_1\partial_r + \zeta_2\partial_\theta + \zeta_3\partial_z)v^3 + (v^1_r + v^2_\theta + v^3_z)\zeta_3 = 0, \tag{3.35}$$

as the terms have clear interpretations. In each equation the first set of terms involves Lie dragging of each vorticity component using $(\partial_t + \mathcal{L}_{\boldsymbol{v}})\zeta_i$, the second set gives vortex stretching via $\mathcal{L}_{\boldsymbol{\zeta}}v^i$ and the final set $(v^1_r + v^2_\theta + v^3_z)\zeta_i$ very roughly corresponds to the intensification of vorticity through compression (bearing in mind that the latter pair of effects are not independent in incompressible flow).

The above Euler and vorticity equations, (3.26–3.29) and (3.33–3.35), are valid for any moving, non-orthogonal coordinate system (r, θ, z). What distinguishes different problems, the actual geometry, resides in the relationships (3.21, 3.23, 3.25). Below we will work to define the (r, θ, z) coordinates so that the vorticity surfaces are given by constant r; at the same time we will derive the motion of the coordinate system given by $\boldsymbol{U}$ and the metric $\boldsymbol{g}$, also μ, to feed into the above framework.

4 Exact formulation for axisymmetric vortex evolution

In this section we shall apply the exact formulation of Euler flows given above to the problem at hand, the evolution of an axisymmetric vortex, as depicted in figure 1(a). There are several choices to be made to facilitate the analysis. The first is the map ϕ from $\mathcal{M}$ to $\tilde{\mathcal{M}}$, taken up in the next subsection. Then we must specify the fluid configuration to be studied, namely a vortex with a circular boundary and a simple choice of axial vorticity and azimuthal velocity as a function of radius. These assumptions will then prepare us for taking the asymptotic slender body limit and making heuristic approximations, together with simulations, as detailed in sections 5 and 6.

4.1 Coordinate system

Recall that we have the vortex evolving in *physical space* $\tilde{\mathcal{M}} = \mathbb{R}^3$, where we mostly use tilde labels, and where we may use Cartesian coordinates $(\tilde{x}, \tilde{y}, \tilde{z})$ or cylindrical polar coordinates $(\tilde{r}, \tilde{\theta}, \tilde{z})$. We will also use Cartesian unit vectors $\boldsymbol{i}$, $\boldsymbol{j}$, $\boldsymbol{k} \equiv \hat{\boldsymbol{z}}$, or for cylindrical polars, $\hat{\boldsymbol{r}}$, $\hat{\boldsymbol{\theta}}$, $\hat{\boldsymbol{z}}$, in $\tilde{\mathcal{M}}$ but without tildes to avoid excessive notation.

The above general development allowed us to exploit coordinates $(x^1, x^2, x^3) = (r, \theta, z)$ in $\mathcal{M}$, as depicted in figure 1(b). These fixed coordinates in $\mathcal{M}$ thus provide moving coordinates in $\tilde{\mathcal{M}}$, through the map ϕ in (3.6). Although the coordinate system is hybrid Eulerian–Lagrangian as mentioned above, we will for brevity refer to the moving coordinates (r, θ, z) as *Lagrangian coordinates*, and we refer to $\mathcal{M}$ as *Lagrangian space*. The coordinate map we use is given by $(\tilde{r}, \tilde{\theta}, \tilde{z}) = \phi(r, \theta, z, t)$ with

$$\tilde{r} = F(r, z, t), \quad \tilde{\theta} = \theta, \quad \tilde{z} = h(z, t), \tag{4.1}$$

where $F(r, z, t)$ and $h(z, t)$ are functions we are free to choose. Note that we set h independent of r, and we require that $F(0, z, t) = 0$ to preserve points on the axis. We will in due course fix the evolution of F and h so that vorticity surfaces are given by constant r and varying z (and θ). The fact that $\tilde{z} = h(z, t)$ is a single-valued function of z means that surfaces will not be able to fold back on themselves, but in any case such folding would violate the slender vortex limit that we will take in due course.

We may use position vectors in Cartesian and polar coordinates in $\tilde{\mathcal{M}}$ to write

$$\tilde{\boldsymbol{r}} = F\cos\theta\,\boldsymbol{i} + F\sin\theta\,\boldsymbol{j} + h\boldsymbol{k} = F\hat{\boldsymbol{r}} + h\hat{\boldsymbol{z}}. \tag{4.2}$$

The velocity of any Lagrangian point is

$$\tilde{\boldsymbol{U}} = \partial_t\tilde{\boldsymbol{r}} = U\hat{\boldsymbol{r}} + W\hat{\boldsymbol{z}}, \tag{4.3}$$

the components being time derivatives of our map,

$$U(r, z, t) = \dot{F}, \quad W(z, t) = \dot{h}. \tag{4.4}$$

Strictly speaking we should write $\tilde{U}$ for U and $\tilde{W}$ for W; however we omit the tildes to keep notation lighter later on. Nonetheless these are velocities in physical space $\tilde{\mathcal{M}}$ referred to the usual unit vectors as in (4.3). We also set

$$J(z, t) = \partial_z h = h', \tag{4.5}$$

so that we have

$$\partial_t J = \partial_z W. \tag{4.6}$$

Here $J(z, t) = \partial\tilde{z}/\partial z$ is the Jacobian of the transformation of points along the axis. We will often use a prime for z-derivatives and a dot for t-derivatives where it is convenient, but we will also use subscripts and ∂_z, ∂_t.

Equation (4.3) gives the velocity of the coordinate system but referred to the unit vectors $\hat{\boldsymbol{r}} = \partial_{\tilde{r}}$ and $\hat{\boldsymbol{z}} = \partial_{\tilde{z}}$: we need to transform these components to the ∂_r and ∂_z coordinate system to obtain the components U^i of $\boldsymbol{U}$ as in (3.25). It may be checked from (4.1) that the change of basis is, explicitly,

$$\begin{pmatrix}\partial_r\\ \partial_z\end{pmatrix} = \boldsymbol{Q}\begin{pmatrix}\partial_{\tilde{r}}\\ \partial_{\tilde{z}}\end{pmatrix}, \quad \begin{pmatrix}\partial_{\tilde{r}}\\ \partial_{\tilde{z}}\end{pmatrix} = \boldsymbol{Q}^{-1}\begin{pmatrix}\partial_r\\ \partial_z\end{pmatrix}, \quad \begin{pmatrix}d\tilde{r}\\ d\tilde{z}\end{pmatrix} = \boldsymbol{Q}^T\begin{pmatrix}dr\\ dz\end{pmatrix}, \quad \begin{pmatrix}dr\\ dz\end{pmatrix} = (\boldsymbol{Q}^{-1})^T\begin{pmatrix}d\tilde{r}\\ d\tilde{z}\end{pmatrix}, \tag{4.7}$$

with

$$\boldsymbol{Q} = \begin{pmatrix} F_r & 0 \\ F_z & h' \end{pmatrix}, \quad \boldsymbol{Q}^{-1} = \begin{pmatrix} F_r^{-1} & 0 \\ -F_z F_r^{-1} h'^{-1} & h'^{-1} \end{pmatrix}. \tag{4.8}$$

For the θ components we simply have $\partial_\theta = \partial_{\tilde{\theta}} = \tilde{r}\hat{\boldsymbol{\theta}}$, $d\tilde{\theta} = d\theta$. Strictly speaking, ∂_r, ∂_z are vectors in $\mathcal{M}$ and $\partial_{\tilde{r}}$, and $\partial_{\tilde{z}}$ are vectors on $\tilde{\mathcal{M}}$, so they cannot be linked in this way! Instead it is the pull-backs $\phi^*\partial_{\tilde{r}}$ and $\phi^*\partial_{\tilde{z}}$ that we are writing in terms of ∂_r, ∂_z. Although we needed the map ϕ to clarify the governing equations in the previous section, in the context of later calculations we generally drop mention of ϕ as the action of the map can be understood in terms of such changes of bases, without undue confusion.

In this way, the components $\tilde{U}^1 = U$ and $\tilde{U}^3 = W$ of the coordinate system velocity $\tilde{\boldsymbol{U}} = \tilde{U}^1\partial_{\tilde{r}} + \tilde{U}^3\partial_{\tilde{z}}$ in the physical space are linked to those in the Lagrangian space, namely $\boldsymbol{U} = U^1\partial_r + U^3\partial_z$, by

$$U^1 = F_r^{-1}U - F_z F_r^{-1} h'^{-1} W = F_r^{-1}\dot{F} - F_z F_r^{-1} h'^{-1}\dot{h}, \quad U^2 = 0, \quad U^3 = h'^{-1}W = h'^{-1}\dot{h}. \tag{4.9}$$

The metric $\boldsymbol{g}$ for the (r, θ, z) coordinate system is calculated from (4.2), by taking the length squared of

$$d\tilde{\boldsymbol{r}} = (F_r\, dr + F_z\, dz)\hat{\boldsymbol{r}} + F\, d\theta\, \hat{\boldsymbol{\theta}} + h'\, dz\, \hat{\boldsymbol{z}}, \tag{4.10}$$

giving

$$\boldsymbol{g} = F_r^2\, dr^2 + F^2\, d\theta^2 + (h'^2 + F_z^2)\, dz^2 + F_r F_z (dr \otimes dz + dz \otimes dr). \tag{4.11}$$

The determinant of the metric tensor is $|\boldsymbol{g}| = F^2 F_r^2 h'^2$ and so we can write the volume form as

$$\boldsymbol{\mu} = \mu\, dr \wedge d\theta \wedge dz, \quad \mu = F F_r h', \tag{4.12}$$

which is the multiple $r^{-1}FF_rh'$ of the usual volume element $r\, dr \wedge d\theta \wedge dz$.

To interpret our coordinates let us set $h' = 1$, say, and then the above transformation in (4.7,4.8) yields

$$\partial_{\tilde{z}}|_{\tilde{r}} = \partial_z|_r - F_z F_r^{-1}\partial_r|_z, \tag{4.13}$$

which relates an axial derivative in the physical space, $\partial_{\tilde{z}}|_{\tilde{r}}$, to an axial derivative in the Lagrangian space, $\partial_z|_r$. A derivative in the Lagrangian space corresponds to a derivative along a vorticity surface in physical space (see figure 1). For the special case of a steady flow this coincides with a derivative along a stream surface, and then (r, z) reduce to von Mises coordinates; this is employed in Klein & Ting (1992) to simplify the PDEs for motion of vortices, steady on the area wave time-scale but evolving on the longer time-scale of vortex motion.

4.2 Vorticity and flow field

Now we need to make choices that define the structure of the vortex and configuration of the moving coordinate system. We will specify that the axial vorticity ζ_3 depends only on

r, that there is no radial vorticity ζ_1, that there is also no radial velocity v^1, and that the configuration is axisymmetric:

$$\zeta_3 = \zeta_3(r), \quad \zeta_1 = 0, \quad v^1 = 0, \quad \partial_\theta = 0. \tag{4.14}$$

This gives the picture with respect to Lagrangian coordinates in figure 1(b), with vortex lines in $\mathcal{M}$ spiralling on fixed cylindrical surfaces, $r = \text{const}$. Naturally the vortex as seen in physical space does possess radial velocity and radial vorticity, as in figure 1(a), and the vorticity surfaces take the form $\tilde{r} = F(r, z, t)$ for $\tilde{z} = h(z, t)$, r fixed and θ, z varying.

With these conditions applied, equations (3.32, 3.33, 3.35) are satisfied automatically, while (3.34) becomes

$$\partial_t \zeta_2 + (v^3 \zeta_2)_z = \zeta_3 \partial_z v^2. \tag{4.15}$$

On the right-hand side is a source term from the wind-up of axial vorticity ζ_3 by the azimuthal flow field v^2, giving azimuthal vorticity ζ_2. In addition, on the left-hand side there is transport of ζ_2 along the axis of the vortex by virtue of the $(v^3\zeta_2)_z$ term. Thus, in the Lagrangian coordinate system, the vorticity dynamics simplifies considerably.

However we have moved much of the complexity to the determination of the moving coordinate system and advecting flow field, and we turn to this now. Equations (3.31) give

$$0 = -\nu_{2z}, \tag{4.16}$$

$$\zeta_2 = \nu_{1z} - \nu_{3r}, \tag{4.17}$$

$$\zeta_3 = \nu_{2r}. \tag{4.18}$$

The first and last of these define $\nu_2(r)$ given $\zeta_3(r)$. We stress here that we are free to choose our vorticity profile $\zeta_3(r)$ to be fixed for all time; the corresponding azimuthal (angular) momentum $\nu_2(r)$ is then also fixed. The actual dynamics is in the other variables.

The profile we choose to use is

$$\zeta_3 = \begin{cases} 2\Omega r, & r \le a, \\ 0, & r > a, \end{cases} \qquad \nu_2 = \begin{cases} \Omega r^2, & r \le a, \\ \Omega a^2, & r > a, \end{cases} \tag{4.19}$$

a Rankine vortex with constant angular velocity Ω, constant radius a and resulting circulation $\Gamma = 2\pi\Omega a^2$ in the Lagrangian coordinates. Note that the full axial vorticity within the vortex is $\zeta_3\, dr \wedge d\theta = 2\Omega r\, dr \wedge d\theta$ and so the vorticity 2Ω per unit area $r\, dr \wedge d\theta$ is uniform. Thus we are choosing the simplest possible vortex core. In physical coordinates the radial extent of the vortex is

$$0 \le \tilde{r} \le \tilde{a}(\tilde{z}, t) \equiv F(a, z, t), \quad \tilde{z} = h(z, t), \tag{4.20}$$

at each $\tilde{z}$ station along the vortex axis; see figure 1(a).

Since the axial $\zeta_3(r)$ vorticity distribution is fixed, it is only the azimuthal component $\zeta_2(r, z, t)$ that has dynamical content. It is this component that drives the advective flow in (4.15), and also evolves the coordinate system in time. To obtain this flow we first note that the incompressibility condition (3.11) or (3.23) permits the introduction of a Stokes stream function ψ given here by

$$(u^1 \partial_r + u^3 \partial_z) \lrcorner \boldsymbol{\mu} = d\boldsymbol{\psi}, \quad \boldsymbol{\psi} = \psi\, d\theta, \tag{4.21}$$

so that

$$u^1 = -(FF_r h')^{-1}\,\psi_z, \quad u^3 = (FF_r h')^{-1}\,\psi_r, \tag{4.22}$$

using the definition of $\boldsymbol{\mu}$ in (4.12). We also have that the momentum $\boldsymbol{\nu} = \boldsymbol{u}_\flat$ is linked to the flow velocity $\boldsymbol{u}$ via (3.21). Using the metric in (4.11) we have for radial and axial components:

$$\nu_1 = F_r^2\,u^1 + F_r F_z u^3, \quad \nu_3 = F_r F_z\,u^1 + (h'^2 + F_z^2)\,u^3. \tag{4.23}$$

(Hopefully from the context there is little risk of confusion between superscripts for squared quantities such as F_r^2 and r^2, and for components u^1, u^2 and u^3.)

Given knowledge of F and h — the shape of the coordinate system — equations (4.17, 4.22, 4.23) combine to give an elliptic second order PDE determining the stream function ψ in terms of the vorticity ζ_2. This needs to be solved with suitable boundary conditions, for example flow decaying as $r \to \infty$ or a prescribed irrotational flow for $r \gg a$, as discussed later. From the solution we obtain the flow components u^1 and u^3, and u^2 is found similarly, via (3.21, 4.11), from

$$\nu_2 = F^2\,u^2. \tag{4.24}$$

In this way we obtain the complete velocity field $\boldsymbol{u}$.

Finally, we need to split the flow $\boldsymbol{u}$ as in (3.25), between motion $\boldsymbol{U}$ of the coordinate system and the residual flow $\boldsymbol{v}$. Recall that our chosen F and h provide $\boldsymbol{U}$ and so determine the splitting $\boldsymbol{u} = \boldsymbol{U} + \boldsymbol{v}$. Conversely, imposing the condition $v^1 = 0$ in (4.14), namely that the coordinate system follows vorticity surfaces, gives a constraint on F and h which we use as an evolution equation for F. From (3.25, 4.9) with $v^1 = 0$, we have

$$u^1 = U^1 = F_r^{-1}\dot{F} - F_z F_r^{-1} h'^{-1}\dot{h}, \tag{4.25}$$

$$u^2 = v^2, \tag{4.26}$$

$$u^3 = U^3 + v^3 = h'^{-1}\dot{h} + v^3. \tag{4.27}$$

In (4.25) the actual radial motion given by u^1 is completely absorbed by the coordinate system, and so (4.25) provides the PDE we need to step $F(r,z,t)$ in time given u^1 and h:

$$\partial_t F = F_r u^1 + F_z h'^{-1}\dot{h}. \tag{4.28}$$

In (4.26) there is no azimuthal motion of the cooordinates so that $U^2 = 0$ and u^2 and v^2 are identical, given by (4.24) with ν_2 as in (4.19): these express angular momentum conservation during the vortex evolution.

We have not yet chosen or constrained the function $h(z,t)$ and this is still open to us, as the remaining freedom in the choice of coordinate system. In the axial component (4.27) this corresponds to a split of the actual velocity $u^3(r,z,t)$ into a piece $U^3(z,t)$ determining the motion of the coordinate system and the residual piece v^3 that appears in the axial advection of vorticity, as in (4.15). Since generally u^3 will have a non-trivial dependence on r there is no unique way to do this and we can make choices depending on the situation. One option, which we use below to study the simplified models, is to take U^3 to be the average axial flow $U^3 = \bar{u}^3$. A simpler option is to take $U^3 = 0$, $\dot{h} = 0$, and say $h(z,t) = z$; in other words we just switch off any axial motion of the coordinate system. We shall take this option for the

numerical runs in section 5. Finally, we can use $h(z,t)$ to adapt the coordinate system to an externally imposed flow, as we do in section 7.

4.3 Vorticity and flow field in physical space

In the Lagrangian coordinate system it is easy to lose track of what the various velocity and vorticity components are in the physical space $\tilde{\mathcal{M}}$ and how these tie up with the calculations in section 2; in this section we make some links. From the vorticity 2-form field $\boldsymbol{\zeta}$ we define the vorticity vector field $\boldsymbol{\omega}$ via $\boldsymbol{\omega} \lrcorner \boldsymbol{\mu} = \boldsymbol{\zeta}$, which yields (see also appendix A),

$$\boldsymbol{\omega} = \omega^1 \partial_r + \omega^2 \partial_\theta + \omega^3 \partial_z, \quad \omega^1 = \mu^{-1}\zeta_1, \quad \omega^2 = \mu^{-1}\zeta_2, \quad \omega^3 = \mu^{-1}\zeta_3. \tag{4.29}$$

Let us focus on ζ_3 and set $\boldsymbol{\omega}_{\text{axial}} = \omega^3 \partial_z$. Using the profile (4.19) and working through the change of basis in (4.7) we obtain inside the vortex

$$\boldsymbol{\omega}_{\text{axial}} = 2\Omega r \mu^{-1} \partial_z = 2\Omega r (F F_r h')^{-1} (F_z \hat{\boldsymbol{r}} + h' \hat{\boldsymbol{z}}). \tag{4.30}$$

Thus while the distribution inside, $\zeta_3 = 2\Omega r$, is fixed, the physical vorticity field can change in magnitude as the coordinate system flexes, and gains a radial as well as an axial component.

This formula (4.30) is general, but if we take a simple situation (as discussed later) in which we have $F = rf(z,t)$ with $f^2 h' = 1$, so that the expansion or contraction in scale by a factor f at each z station is uniform, then this simplifies to

$$\boldsymbol{\omega}_{\text{axial}} = 2\Omega (r f' \hat{\boldsymbol{r}} + h' \hat{\boldsymbol{z}}) = \frac{\Gamma}{A} \left(\frac{r f'}{h'} \, \hat{\boldsymbol{r}} + \hat{\boldsymbol{z}} \right), \tag{4.31}$$

where we identify $A = \pi \tilde{a}^2 = \pi a^2 f^2$ and use the circulation $\Gamma = 2\pi\Omega a^2$. The $\hat{\boldsymbol{z}}$ component here is Γ/A as we had in (2.11). Likewise we can consider the component of the momentum ν_2 and set $\boldsymbol{\nu}_{\text{azi}} = \nu_2 \, d\theta = \nu_2 \, d\tilde{\theta}$. The corresponding velocity component is $\boldsymbol{u}_{\text{azi}} = \boldsymbol{\nu}_{\text{azi}\sharp} = \tilde{r}^{-2} \nu_2 \partial_{\tilde{\theta}} = \tilde{r}^{-1} \nu_2 \hat{\boldsymbol{\theta}}$, thus giving for the profile (4.19) (as $\tilde{r} = rf$, $\tilde{a} = af$),

$$\boldsymbol{u}_{\text{azi}} = \begin{cases} \Omega r^2 \tilde{r}^{-1} \hat{\boldsymbol{\theta}} = \Gamma \tilde{r} / 2A \, \hat{\boldsymbol{\theta}}, & \tilde{r} \le \tilde{a}, \\ \Omega a^2 \tilde{r}^{-1} \hat{\boldsymbol{\theta}} = \Gamma / 2\pi \tilde{r} \, \hat{\boldsymbol{\theta}}, & \tilde{r} > \tilde{a}, \end{cases} \tag{4.32}$$

in agreement with (2.12). Finally, while the profiles in (4.19) are fixed for all time, ζ_2 evolves according to (4.15). Below we consider a simplified model with $\zeta_2 = r\chi(z,t)$, in (6.6); here this corresponds to $\omega^2 = \mu^{-1} r \chi(z,t)$ from (4.29), and (again with $F = rf$, $f^2 h' = 1$, $\mu = r$) we have

$$\boldsymbol{\omega}_{\text{azi}} = \omega^2 \partial_\theta = \omega^2 \partial_{\tilde{\theta}} = \chi \partial_{\tilde{\theta}} = \tilde{r} \chi \hat{\boldsymbol{\theta}}, \tag{4.33}$$

in agreement with (2.19). Thus the notation and fields are consistent when comparing the present Lagrangian model with the discussion in section 2.

5 Slender vortex limit

5.1 Slender vortex scalings

The system as outlined in the previous section is a complete Lagrangian description of the evolution of a vortex under only the assumption of axisymmetry. Naturally, adopting a flexible coordinate system means unavoidable complexity in the elliptic problem that would need to be solved numerically to go from ζ_2 to ψ. Thus, this approach offers few advantages over an Eulerian description. We therefore revisit the limit of a slender vortex introduced in section 2, using now the notation of the Lagrangian description.

In Lagrangian space our vortex sits in $0 \le r \le a$ and $0 \le z \le \ell$ with, say, periodic boundary conditions in z. Let us take $a = O(1)$ and $\ell \gg 1$. We have freedom in the fundamental design of the map ϕ, so we use it to map the vortex in $\mathcal{M}$ to a vortex in $\tilde{\mathcal{M}}$ of similar proportions, with radius and length

$$\tilde{a}(\tilde{z},t) = F(a,z,t) = O(1), \quad \tilde{\ell}(t) = h(\ell,t) - h(0,t) = O(\ell). \tag{5.1}$$

The slender vortex scalings are

$$F = O(1), \quad h = O(\ell), \quad \partial_r = O(1), \quad \partial_z = O(\ell^{-1}), \quad \partial_t = O(\ell^{-1}). \tag{5.2}$$

For the flow variables the appropriate scalings are

$$\zeta_2 = O(1), \quad \zeta_3 = O(1), \quad u^1, v^1, U^1 = O(\ell^{-1}), \quad u^2, v^2, u^3, v^3, U^3 = O(1), \tag{5.3}$$

$$\psi = O(1), \quad \nu_1 = O(\ell^{-1}), \quad \nu_2, \nu_3 = O(1), \quad p = O(1) \tag{5.4}$$

(pressure p will be mentioned later). Then (4.17) and (4.23b) simplify to

$$\zeta_2 = -\nu_{3r}, \quad \nu_3 = h'^2 u^3, \tag{5.5}$$

at leading order. With these and (4.22), the elliptic problem for ψ given ζ_2 simplifies down to an equation involving only r-derivatives,

$$\zeta_2 = -[(FF_r)^{-1} h' \psi_r]_r \tag{5.6}$$

(cf. (2.2) in the Eulerian description). Solutions to the homogeneous form of (5.6) take the form $\psi = \gamma(z,t)F^2 + \delta(z,t)$. The term δ must be excluded as $r \to 0$ since the corresponding flow obtained from (4.22) is singular there. The $\gamma F^2 = \gamma \tilde{r}^2$ piece grows as $\tilde{r} \to \infty$ and so must be excluded for $r > a$ as there is (for the time being) no externally imposed irrotational flow, giving the boundary condition

$$\partial_r \psi|_{r=a} = 0, \tag{5.7}$$

corresponding to zero axial flow u^3 at $r = a$. The evolution is given by time-stepping the PDE (4.15) for ζ_2 with (5.6) used to calculate ψ and so u^1, u^3 from (4.22) and then use made of (4.24–4.27) as before. This remains a system in (r,z,t) variables which can only generally be tackled numerically, as we proceed to do.

5.2 Numerical solution

We now outline the basis of our numerical solution of area waves in the slender vortex system. The solution to (5.6) under the boundary conditions discussed above is (suppressing the dependence on z, t),

$$\psi(r) = \tfrac{1}{2} h'^{-1} \left[\int_0^r F(\rho)^2 \, \zeta_2(\rho) \, d\rho + F(r)^2 \int_r^a \zeta_2(\rho) \, d\rho \right], \tag{5.8}$$

and so

$$u^3(r) = h'^{-2} \int_r^a \zeta_2(\rho) \, d\rho. \tag{5.9}$$

For the numerical solution we make the choice that $h(z,t) = z$, as indicated at the end of section 4.2, which removes any axial motion of the coordinate system from consideration, and makes $h' = 1$, $\dot{h} = 0$, $U^3 = 0$. Other choices here would simply give the same results under an axial coordinate transformation: for example, in section 6.1 we average the axial flow to obtain the vorticity wave model, and then a different choice of h is convenient. Starting with a vortex profile in (4.19), we then have two PDEs to time step, namely (4.15) for the azimuthal vorticity $\zeta_2(r,z,t)$, and

$$\partial_t F = F_r \, u^1 \tag{5.10}$$

for the shape of vorticity surfaces from (4.28), together with the use of the relationships

$$u^1 = -(F F_r)^{-1} \psi_z, \quad u^2 = v^2 = F^{-2} \nu_2, \quad u^3 = v^3 = (F F_r)^{-1} \psi_r, \tag{5.11}$$

and (5.8, 5.9) with $h' = 1$.

It is convenient for numerical solution to introduce an area variable $\alpha(r,z,t) = F^2$ so that the physical cross-sectional vortex area is $\pi\alpha(r,z,t)$ at each value of r and axial location $z = \tilde{z}$. With this the evolution equations take a convenient conservation form,

$$\partial_t \zeta_2 = (v^2 \zeta_3 - v^3 \zeta_2)_z, \quad \partial_t \alpha = -2\psi_z, \tag{5.12}$$

with

$$v^2 = \alpha^{-1} \nu_2, \quad v^3 = \int_r^a \zeta_2(\rho) \, d\rho, \quad \psi = \tfrac{1}{2} \left[\int_0^r \alpha(\rho) \, \zeta_2(\rho) \, d\rho + \alpha(r) \int_r^a \zeta_2(\rho) \, d\rho \right]. \tag{5.13}$$

The equations are integrated numerically using a Lax–Wendroff scheme with 200 points in r and z.

5.3 Numerical results

Having chosen a base vorticity profile as say (4.19), the remaining parameters are (a, Ω, ℓ) giving also the circulation $\Gamma = 2\pi\Omega a^2$. We are free to choose the scale a and angular velocity (inverse time) scale Ω, in effect to non-dimensionalise the equations on this basis. In line with later non-dimensionalisation of the vorticity and area wave models, we will without loss of

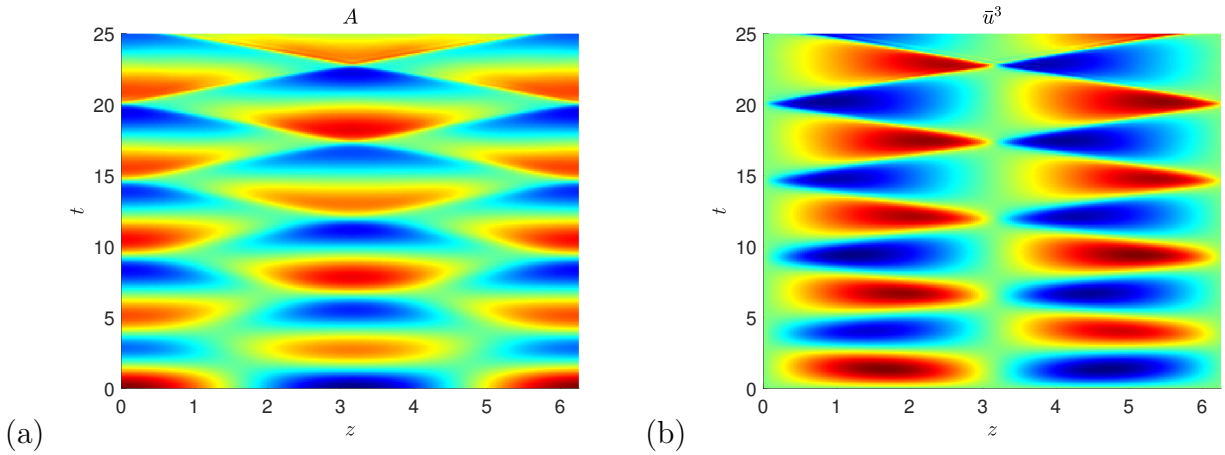

Fig. 2. Slender vortex simulations for the initial $A(z,0)$ in (5.16) and $\bar{u}^3(z,0) = W_0 = 0$: (a) A (from 0.9π to 1.1π) and (b) $\bar{u}^3$ (from -0.87 to 0.87) are depicted on a colour scale in the (z,t)-plane with here $z = \tilde{z}$.

generality fix a and Ω with:

$$a = 1, \quad \Omega = \sqrt{2}, \quad \Gamma = 2\pi\sqrt{2}. \tag{5.14}$$

We also fix the period of any wave as $\ell = 2\pi$ without loss of generality: the slender vortex theory is valid in the limit $\ell \to \infty$ so in practice we have scaled ℓ out of the problem via (5.2–5.4) and are thus able to fix it arbitrarily.

To compare with the vorticity and momentum wave models we will focus on plots of the area profile $A(z,t)$ of the vortex, setting

$$A(z,t) = \pi\tilde{a}^2(z,t) = \pi\alpha(a,z,t) = \pi F^2(a,z,t). \tag{5.15}$$

To start a wave in the simulation we specify a variation in area, and take

$$A(z,0) = \pi(A_0 + A_{01}\cos z), \quad F(r,z,0) = r(A_0 + A_{01}\cos z)^{1/2}, \quad A_0 = 1, \quad A_{01} = 0.1, \tag{5.16}$$

a uniform contraction/expansion at each z station. The other key quantity is some measure of the axial flow. Now this component is $u^3\,\partial_z = u^3\,\partial_{\tilde{z}} = u^3\,\hat{\boldsymbol{z}}$ (as $h' = 1$ here), but as $u^3 = u^3(r,z,t)$ this generally depends on radius. To compare with the axial flow $W(z,t)$ in the vorticity and area wave models we use the average of u^3 over the vortex, setting

$$\bar{u}^3(z,t) = \langle u^3 \rangle \equiv \frac{1}{\pi\tilde{a}^2}\int_0^{\tilde{a}} u^3\, 2\pi\tilde{r}\, d\tilde{r} = \frac{2}{\tilde{a}^2}\int_0^{a} u^3 F F_r\, dr = \frac{1}{\tilde{a}^2}\int_0^{\tilde{a}^2} u^3\, d\alpha. \tag{5.17}$$

We also need to be able to impose an initial axial flow corresponding to a given $W(z,t)$, in other words impose an initial $\bar{u}^3(z,0)$. For this we will choose a quadratic profile by setting

$$\zeta_2(r,z,0) = 4a^{-2}r\,\bar{u}^3(z,0), \quad u^3(r,z,0) = 2a^{-2}(a^2 - r^2)\,\bar{u}^3(z,0), \tag{5.18}$$

as per (5.9).

Results from the numerical simulations are presented in figures 2–5. The first figure shows evolution of the initial area profile in (5.16) and zero initial axial flow, $\bar{u}^3 = W_0 = 0$ in (5.18). in

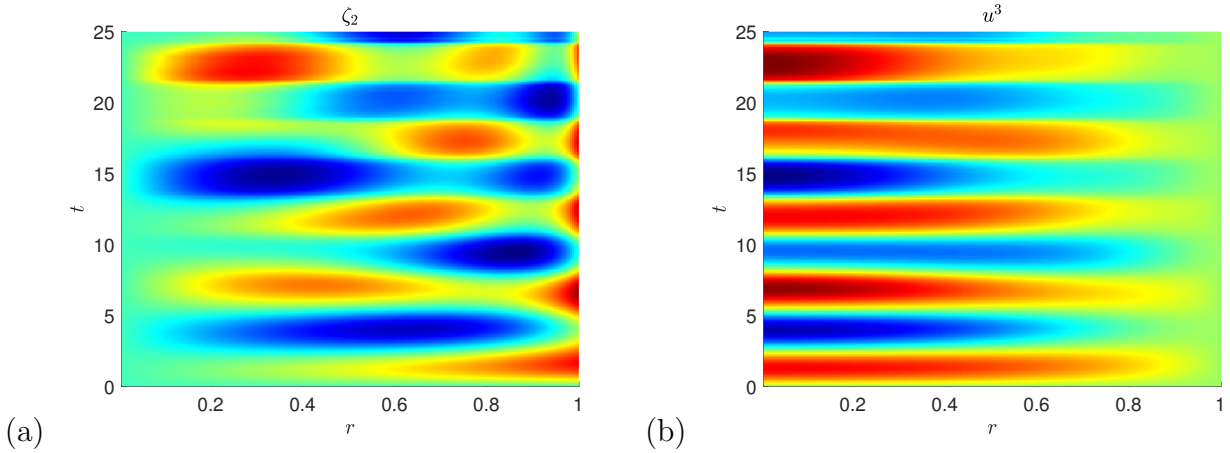

Fig. 3. Slender vortex simulations for the initial $A(z,0)$ in (5.16) and $\bar{u}^3(z,0) = W_0 = 0$: (a) ζ_2 (from -0.42 to 0.53) and (b) u^3 (from -0.24 to 0.22) are depicted on a colour scale in the (r,t)-plane for $z = \pi/2$ and $z = \pi/4$ respectively.

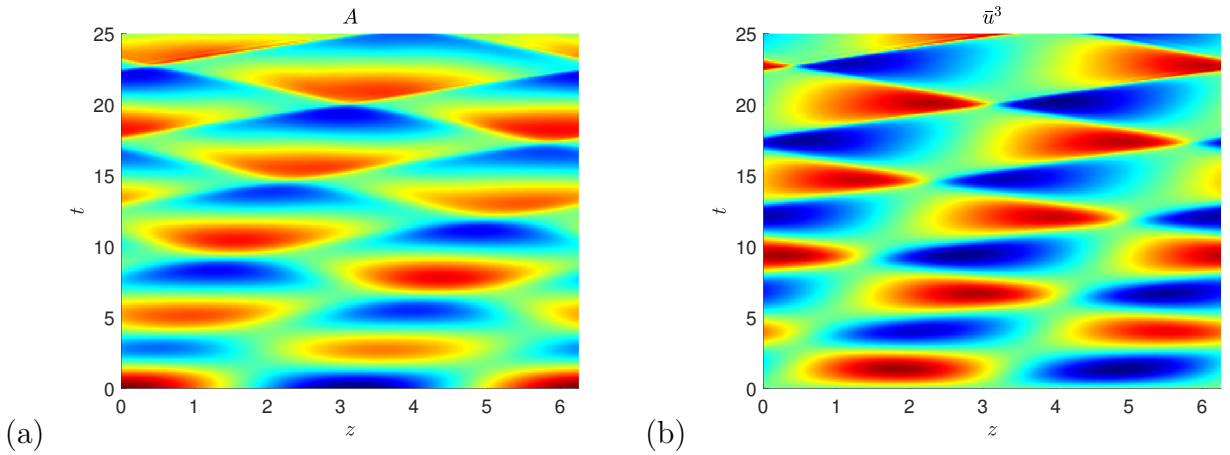

Fig. 4. Slender vortex simulations for the initial $A(z,0)$ in (5.16) and $\bar{u}^3(z,0) = W_0 = 0.1$: (a) A (from 0.9π to 1.1π) and (b) $\bar{u}^3$ (from 0.013 to 0.188) are shown in the (z,t)-plane with here $z = \tilde{z}$.

the (z,t) plane with time running up to $t = 25$. The evolution of A is shown in panel 2(a) and the mean axial flow $\bar{u}^3$ in panel 2(b). We observe a standing pattern of waves: axial flow runs from thick to thin regions of the vortex, overshoots and then goes back again. As one might expect in this hyperbolic system with no dissipation, the wave forms tend to sharpen and form shock-like structures in the later evolution. To illustrate the internal vortex structure figure 3(a) shows ζ_2 at the $z = \pi/2$ station with radius r horizontal and time up to $t = 25$ vertically. This field gains a structure of nested, like-signed rings, more complicated than the simplified profile that we use for the vorticity wave model in (6.6) below, which is linear, proportional to r. On the other hand the resulting axial flow, shown in figure 3(b) at $z = \pi/4$, retains a reasonable approximation to a quadratic profile throughout the run, until small scales from shock behaviour appear. The overall pattern of standing waves does not propagate in (z,t) space, by virtue of the $z \to -z$ symmetry of the equations and initial conditions. Because of our choice of h, we have $\tilde{z} = z$ and so the figures are the same with respect to physical and Lagrangian axial coordinates. Note that the $W = 0$ case is the classic Rankine vortex, which is known to be neutrally stable, including a long-wavelength axisymmetric wave propagating with a speed of around $\pm 0.835\Omega a \simeq \pm 1.18$ (see, e.g. Saffman, 1992), giving good agreement with the period of the standing waves in figure 2.

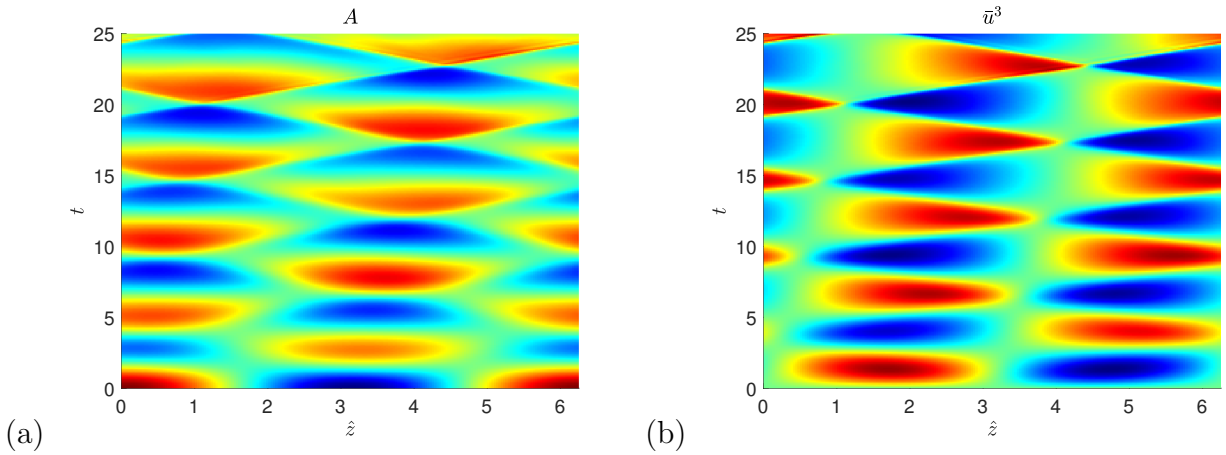

Fig. 5. Slender vortex simulations for the initial $A(z,0)$ in (5.16) and $\bar{u}^3(z,0) = W_0 = 0.1$: (a) A (from 0.9π to 1.1π) and (b) $\bar{u}^3$ (from 0.013 to 0.188) are shown in the $(\hat{z},t)$-plane, $\hat{z} = z - W_0 t$.

Next we introduce a non-zero initial axial flow, a constant $\bar{u}^3(z,0) = W_0 = 0.1$, giving the azimuthal vorticity ζ_2 and axial flow u^3 specified by (5.18). Figure 4 shows the quantities A and $\bar{u}^3$ in the (z,t)-plane, showing a similar pattern, now propagating to the right. To compare with later simulations we also show the same panels in figure 5, now plotted in the $(\hat{z},t)$ plane where $\hat{z} = z - W_0 t$ is a Lagrangian coordinate following the mean flow (noting that $\bar{u}^3$ averaged over z remains at $W_0 = 0.1$ for this run). The standing wave pattern continues to propagate to the right, with respect to the mean axial flow.

6 The vorticity and momentum wave models

6.1 Assumptions and derivation

We now seek to compare our numerical results with the simplified models in which we remove the radial dependence from the full slender vortex system above. Within our Lagrangian framework we will first derive the vorticity wave model, which as discussed in section 2 is based on vorticity conservation in L94, as distinguished from the momentum wave model of LA89. We will thus make two key *modelling assumption*s that will prove not to be justified, but when an averaging step is put it in, will yield the vorticity wave model that we derived in the Eulerian framework in section 2.

Our first modelling assumption is that the vorticity surfaces are such that there is only a uniform compression or expansion of the coordinate system at each z-station, so that we replace the general $F(r,z,t)$ by the specific form

$$F(r,z,t) = r f(z,t). \tag{6.1}$$

This restricts the allowed geometry of the vortex surfaces. With (6.1) we will make use of our freedom to choose the flow of the coordinate system in the z-direction by making the convenient requirement that $h(z,t)$ is to satisfy

$$f^2 h' = 1. \tag{6.2}$$

Once we impose this, we can fix the evolution of f or of h but not both. We will shortly focus on allowing h' to match the axial flow. This condition makes the map ϕ from Lagrangian (r, z) to physical $(\tilde{r}, \tilde{z})$ coordinates volume-preserving, with $FF_r h' = rf^2 h' = r$ and so

$$\boldsymbol{\mu} = \mu \, dr \wedge d\theta \wedge dz, \quad \mu = r, \tag{6.3}$$

from (4.12). With this, (4.22) is replaced by

$$u^1 = -r^{-1}\psi_z, \quad u^3 = r^{-1}\psi_r. \tag{6.4}$$

We will take uniform axial vorticity ζ_3 in the vortex, as per (4.19) (other choices could be made), and consider the governing equation (4.15) for the azimuthal vorticity ζ_2. Our second modelling assumption is that the advecting axial velocity u^3 that appears in the vorticity equation (4.15) is a uniform 'slug flow', [3] independent of r across the vortex $r \le a$. This means that using $u^3 = U^3 + v^3$ we can absorb the axial flow completely into the coordinate system $u^3 = U^3(z,t)$, $v^3 = 0$ giving the evolution of $h(z,t)$ as in (4.27). With $v^3 = 0$, equation (4.15) simplifies to

$$\partial_t \zeta_2 = \zeta_3 \, \partial_z v^2, \tag{6.5}$$

with $v^2 = u^2 = \Omega f^{-2}$ from (4.19, 4.24, 6.1). The solution to this may be written as

$$\zeta_2(r, z, t) = \chi(z, t) r, \qquad r \le a, \tag{6.6}$$

and zero for $r > a$, with

$$\partial_t \chi = 2\Omega^2 \, \partial_z f^{-2}. \tag{6.7}$$

This represents the generation of azimuthal vorticity ζ_2 by variations in the local angular velocity v^2 along the vortex. It arises from the variation of area in z and so ultimately by conservation of angular momentum. The cross-sectional area $A(z,t)$ in (5.15) is now given by

$$A(z, t) = \pi a^2 f^2(z, t). \tag{6.8}$$

The azimuthal vorticity ζ_2 in (6.6) is now a source of axial and radial flow, via the stream function ψ. We need to integrate out the relation (5.6) which is

$$(r^{-1}\psi_r)_r = -\chi f^4 r, \qquad r \le a, \tag{6.9}$$

and zero for $r > a$. This has the homogeneous solution (cf. discussion above (5.8)) $\psi = \gamma(z,t) r^2 + \delta(z,t)$ and with this we obtain, for a flow that is regular at $r = 0$ and dies away as $r \to \infty$,

$$\psi = \begin{cases} -\frac{1}{8}\chi f^4 r^2 (r^2 - 2a^2), \\ \frac{1}{8}\chi f^4 a^4, \end{cases} \quad u^1 = \begin{cases} \frac{1}{8}(\chi f^4)' r (r^2 - 2a^2), \\ -\frac{1}{8}(\chi f^4)' a^4 r^{-1}, \end{cases} \quad u^3 = \begin{cases} -\frac{1}{2}\chi f^4 (r^2 - a^2), & r \le a, \\ 0, & r > a. \end{cases} \tag{6.10}$$

We can now assess what we have in view of the earlier modelling assumptions, that the vorticity surfaces take a simple form and the axial flow is independent of r. Our first assumption was

[3] Note that if the vorticity surfaces are given by a uniform expansion/contraction for each z in (6.1), this geometry is preserved if the axial flow is independent of r.

invoked to simplify $F(r,z,t) = rf(z,t)$ in (6.1) so that at each z-station the coordinate system expands or contracts uniformly in r. For this to be correct the flow $u^1 = U^1$ above needs to be strictly linear in r, and we observe that it isn't. Similarly the second assumption requires the axial velocity u^3 to be uniform in radius so that we can set $u^3 = U^3(z,t)$ only and $v^3 = 0$. Again this does not hold: the winding up of uniform axial vorticity creates an azimuthal vorticity component ζ_2 that gives a quadratic axial flow profile u^3.

To eliminate radial dependence we must take a heuristic step. As we have started by assuming a uniform axial flow $u^3 = U^3(z,t)$, independent of radius, in writing down (6.5), the most straightforward step to take is to replace the u^3 that appears in the vorticity equation (6.5) by its average $\bar{u}^3$ (averaged with respect to area $r\,dr \wedge d\theta$) and set $U^3 = \bar{u}^3$, $v^3 = 0$. This fixes the evolution of the geometry, with

$$U^3 = \dot{h}/h' = f^2\dot{h} = \bar{u}^3 = \tfrac{1}{4}\chi f^4 a^2. \tag{6.11}$$

Then our closed system of equations is

$$\partial_t \chi = 2\Omega^2 \partial_z f^{-2}, \quad \partial_t h = \tfrac{1}{4}\chi f^2 a^2, \quad f^2 \partial_z h = 1. \tag{6.12}$$

Gathering up elements from elsewhere, namely $W = \dot{h}$, $J = h'$, $\Gamma = 2\pi\Omega a^2$, $A = \pi a^2 f^2$ and eliminating $\chi = 4\pi W/A$, we obtain a closed set of equations as

$$A\,\partial_t\left(\frac{W}{A}\right) = \frac{\Gamma^2}{8\pi J}\,\partial_z\left(\frac{1}{A}\right), \quad \partial_t J = \partial_z W, \quad AJ = \pi a^2. \tag{6.13}$$

These are the governing equations in Lagrangian coordinates for the vorticity wave model. A similar system is obtained by L94 (with different constants that arise from different weighting in the averages). Again we stress that while W appears prominently in the equation, this is fundamentally an equation governing azimuthal vorticity, here measured by $\chi = 4\pi W/A$.

We leave the equation in the above form for easy comparison with the momentum wave model (2.18) of LA89, which in Lagrangian coordinates amounts to

$$\partial_t W = \frac{\Gamma^2}{8\pi J}\,\partial_z\left(\frac{1}{A}\right), \quad \partial_t J = \partial_z W, \quad AJ = \pi a^2. \tag{6.14}$$

Our discussion using geometrical tools is based on following vorticity surfaces, and a derivation of the LA89 model, based as it is on averaging the Euler or momentum equation, does not fit so naturally into this framework. Nonetheless we check in appendix B that the LA89 model may be obtained from the Euler equation written in the form given in section 3.

Going from Lagrangian to Eulerian variables we have the relationships:

$$\partial_t = \partial_{\tilde{t}} + W\partial_{\tilde{z}}, \quad \partial_z = J\partial_{\tilde{z}} = \pi a^2 A^{-1}\partial_{\tilde{z}}, \tag{6.15}$$

and the system (6.13) becomes (2.26), while (6.14) beomes (2.18), as derived in section 2 (with appropriate substitution $(\tilde{z},\tilde{t}) \to (z,t)$).

In the discussion below (6.2) we explained that we could fix the evolution of f or of h' to close the system, but not generally both. It is interesting to check the outcome if we followed

an alternative approach, say to set $U^1(a,z,t) = u^1(a,z,t) = -\frac{1}{8}(\chi f^4)'a^3$ so that the evolution of f now tracks the motion of the boundary $r = a$, $\tilde{r} = \tilde{a}$ of the vortex; a short calculation leads to the same system of equations. Specifically we use (4.28, 6.10)

$$U^1(a,z,t) = u^1(a,z,t) = -\tfrac{1}{8}(\chi f^4)'a^3 = a(\dot{f}/f - \dot{h}f'/h'f) = -\tfrac{1}{2}a(\dot{h}/h')', \tag{6.16}$$

with $f^2h' = 1$ giving $\dot{f}/f = -\frac{1}{2}\dot{h}'/h'$ and $f'/f = -\frac{1}{2}h''/h'$. Integrating implies that

$$\dot{h}/h' = \tfrac{1}{4}\chi f^4 a^2, \tag{6.17}$$

up to a constant $C(t)$ of integration which we set to zero (it would correspond to adding a uniform flow in the axial direction). Thus it turns out that we recover (6.11), and on hindsight this follows from conserving the volume of the vortex in physical space. The two choices of evolving h or evolving f amount to the same final answer in this case, though other choices, for example taking other profiles with the same circulation and/or another weighted average of the axial flow, could give other constants in the equations: these are members of a general class of approximate models, pioneered in L94.

6.2 Numerical simulations

We will simulate the equations for the momentum and vorticity wave models numerically to compare with the slender vortex system. First we non-dimensionalise, following discussion in LA89 (section 4) and set a length scale, area scale and time scale via

$$\mathcal{L} = a, \quad \mathcal{A} = \pi a^2, \quad \mathcal{T} = 2\sqrt{2}\pi a^2/\Gamma. \tag{6.18}$$

Note that the time taken for a particle to go around the circumference of a vortex radius a, circulation Γ, is $\sqrt{2}\mathcal{T}$; the velocity scale $\mathcal{L}/\mathcal{T}$ is the maximum velocity in the vortex (i.e. at $r = a$), divided by $\sqrt{2}$. We set, using daggers temporarily to denote new dimensionless variables,

$$z = \mathcal{L}z^\dagger, \quad t = \mathcal{T}t^\dagger, \quad A = \mathcal{A}A^\dagger, \quad W = (\mathcal{L}/\mathcal{T})W^\dagger, \quad J = J^\dagger, \quad h = \mathcal{L}h^\dagger, \tag{6.19}$$

to leave, dropping the daggers, for the vorticity wave model (6.13),

$$A\,\partial_t\left(\frac{W}{A}\right) = -\partial_z \log A, \quad \partial_t J = \partial_z W, \quad AJ = 1, \tag{6.20}$$

and for the momentum wave model (6.14),

$$\partial_t W = -\partial_z \log A, \quad \partial_t J = \partial_z W, \quad AJ = 1. \tag{6.21}$$

This non-dimensionalisation corresponds to the choice of values in (5.14) for simulations of the slender vortex system (though the area A there is π times the area here), and this allows direct comparison of numerical results.

We present numerical simulations of the two models: these were written in conservation form for Lax–Wendroff time stepping using the following pairs of variables and equations as

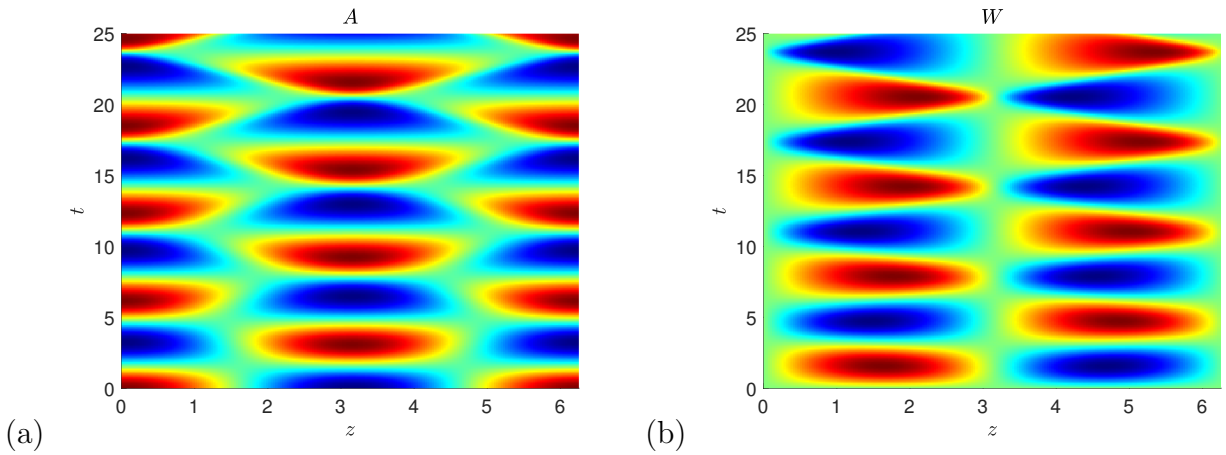

Fig. 6. Momentum wave simulations for the initial $A(z,0)$ in (5.16) and $W(z,0) = W_0 = 0$: (a) A (from 0.9 to 1.1) and (b) W (from -0.1 to 0.1) are depicted on a colour scale in the (z,t)-plane. The figure also applies for other values of W_0, with W plotted in the range $-0.1 + W_0$ to $0.1 + W_0$ in (b).

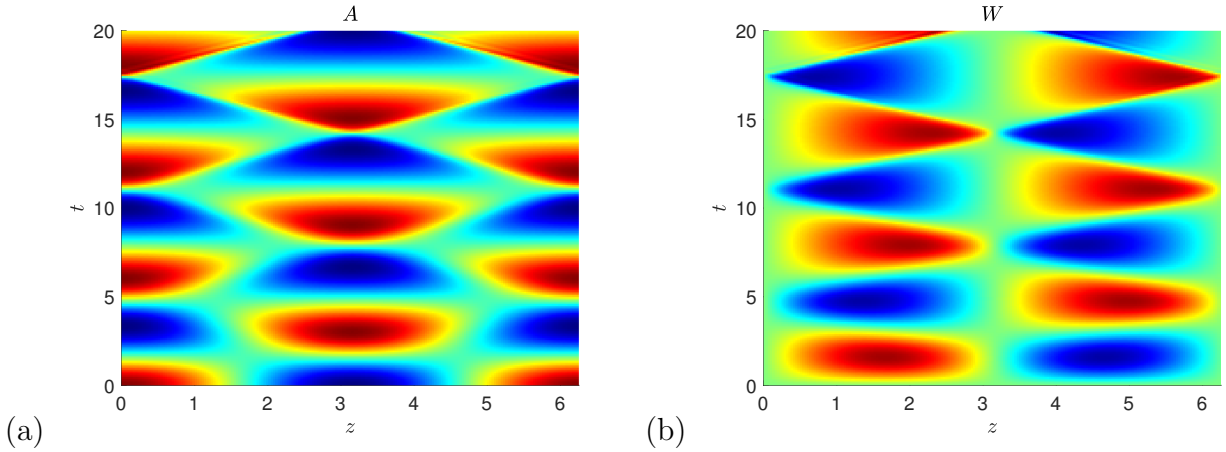

Fig. 7. Vorticity wave simulations for the initial $A(z,0)$ in (5.16) and $W(z,0) = W_0 = 0$: (a) A (from 0.9 to 1.1) and (b) W (from -0.11 to 0.11) are depicted on a colour scale in the (z,t)-plane.

follows

$$\text{momentum wave:} \quad (W,J): \qquad \partial_t W = \partial_z \log J, \quad \partial_t J = \partial_z W, \tag{6.22}$$

$$\text{vorticity wave:} \quad (WJ,J): \qquad \partial_t (WJ) = \partial_z J, \quad \partial_t J = \partial_z (J^{-1}(WJ)). \tag{6.23}$$

For the LA89 momentum wave model, figure 6 shows numerical results with $W(z,0) = W_0 = 0$ and the initial area profile $A(z,0) = A_0 + A_{01}\cos z$, $A_0 = 1$, $A_{01} = 0.1$; see (5.16). Figure 7 shows simulations for the vorticity wave model but only up to $t = 20$, as soon after this the steepening of the wave motion does not allow further computation. The results of both of these are similar and may be compared with those for the full slender system in figure 2, which shows a comparable pattern of waves up to $t = 25$, with slightly shorter period, i.e. the waves are a little more vigorous.

We then keep the same initial $A(z,0)$ but set a constant initial axial flow $W(z,0) = W_0 \neq 0$. Before showing any results it is worth considering symmetries of the equations. Naturally both vorticity and momentum models, and the exact slender vortex system, have the symmetry of

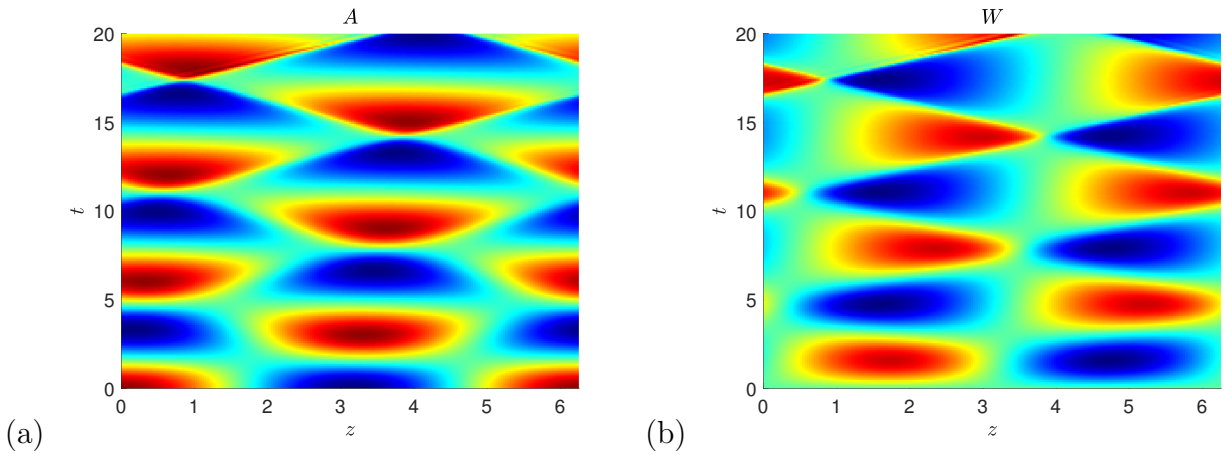

Fig. 8. Vorticity wave simulations for the initial $A(z,0)$ in (5.16) and $W(z,0) = W_0 = 0.1$: (a) A (from 0.9 to 1.1) and (b) W (from 0 to 0.22) are shown in the (z,t)-plane, z being the Lagrangian coordinate.

reversing the axial flow and the axial direction,

$$W(z,t) \to -W(-z,t), \quad A(z,t) \to A(-z,t), \tag{6.24}$$

giving the motionless standing waves in figures 2, 6, 7 when the initial condition has $W = 0$ and A even in z. However, in addition the LA89 momentum wave model is unchanged when

$$W(z,t) \to W(z,t) + C, \quad A(z,t) \to A(z,t), \tag{6.25}$$

where C is any constant. Thus the results for an initial condition with any constant $W = W_0$ are essentially the same as for $W = W_0 = 0$ and the same A. The momentum wave model is blind to Galilean shifts in the velocity inside the vortex. Thus the pictures in figure 6 apply to any initially constant $W = W_0$, with just a shift of the scale in panel (b): the pattern of standing waves does not propagate as we are in a Lagrangian frame (z,t) translating with the mean flow W_0 in the vortex.

However the picture is different for the vorticity wave model (and also for the slender vortex system), since the symmetry (6.25) does not hold and so the results for $W_0 \neq 0$ are intrinsically different from those depicted for $W_0 = 0$ in figure 7. For $W_0 = 0.1$, figure 8 shows evolution of W and A: the standing waves now have a drift on top of the translation in the mean flow. When the results for the same initial conditions in the slender vortex system are referred to the mean flow, in figure 5, we again see the pattern of waves moving rightwards and so the results are close to the vorticity wave model (noting that the horizontal axes in figures 5, 6 and 8 are all essentially equivalent). Again the waves in figure 5 are somewhat more vigorous but otherwise have a similar structure.

The earlier figures show (drifting) patterns of standing waves that are plainly a combination of two waves propagating upstream and downstream. To try to isolate these waves we focus on the dispersion relation for the vorticity wave model, which in the present (z,t) coordinate system (i.e. with z a Lagrangian coordinate moving with the mean flow) is

$$\omega/k = \tfrac{1}{2}W_0 \pm \tfrac{1}{2}\sqrt{W_0^2 + 4}, \tag{6.26}$$

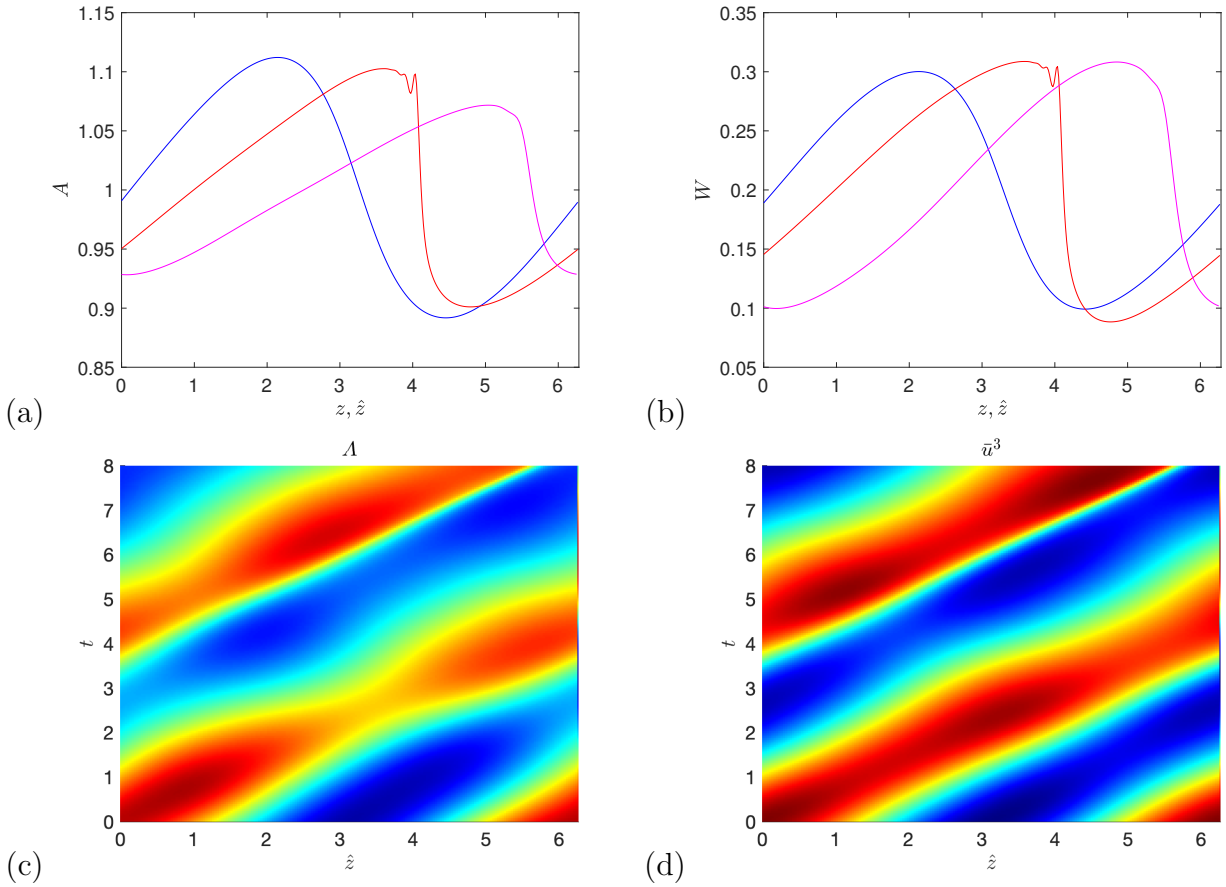

Fig. 9. Downstream wave. Profiles of (a) A and (b) W or $\bar{u}^3$ are plotted against $z \equiv \hat{z}$ at time $t = 8$, in the momentum wave model (blue), vorticity wave model (red) and slender vortex system (magenta). In (c,d) the evolution of A and $\bar{u}^3$ respectively are shown for the slender vortex system in the $(\hat{z}, t)$ plane.

for modes proportional to $e^{ikz-i\omega t}$. We take the initial condition with $A(z,0)$ given in (5.16) and

$$W(z,0) = \bar{u}^3(z,0) = W_0 + W_{01}\cos z, \;\; A_0 = 1, \;\; A_{01} = 0.1, \;\; W_0 = 0.2, \;\; W_{01} = \omega A_{01}/kA_0, \quad (6.27)$$

so the initial condition satisfies the linear dispersion relation for the vorticity wave model. We have also run using the dispersion relation $\omega/k = \pm 1$ appropriate to the momentum wave model, and obtained very similar results, unsurprisingly for this modest value of W_0.

Figure 9 shows the downstream wave (+ sign in (6.26)), with panels (a,b) showing profiles of $A(z,t)$ and $\bar{u}^3(z,t)$ at time $t = 8$. The wave in the full slender vortex system (magenta) has overtaken the waves for the momentum wave model (blue) and vorticity wave model (red). The time $t = 8$ is just before the breaking of the wave in the slender vortex system, while the wave for the vorticity wave model has just broken. The evolution of the fields A and $\bar{u}^3$ in panels (c,d), for the slender vortex system, shows rather more structure than a simple wave. Similarly figure 10 shows the upstream wave ($-$ sign in (6.26)): again the slender vortex system wave is the speediest, and the waves are slower to break. All profiles here are referred to the mean flow, using the coordinates z or $\hat{z}$. Overall the vorticity wave model gives the closest profiles to the full slender vortex system, under a phase shift, although it underestimates the velocity of

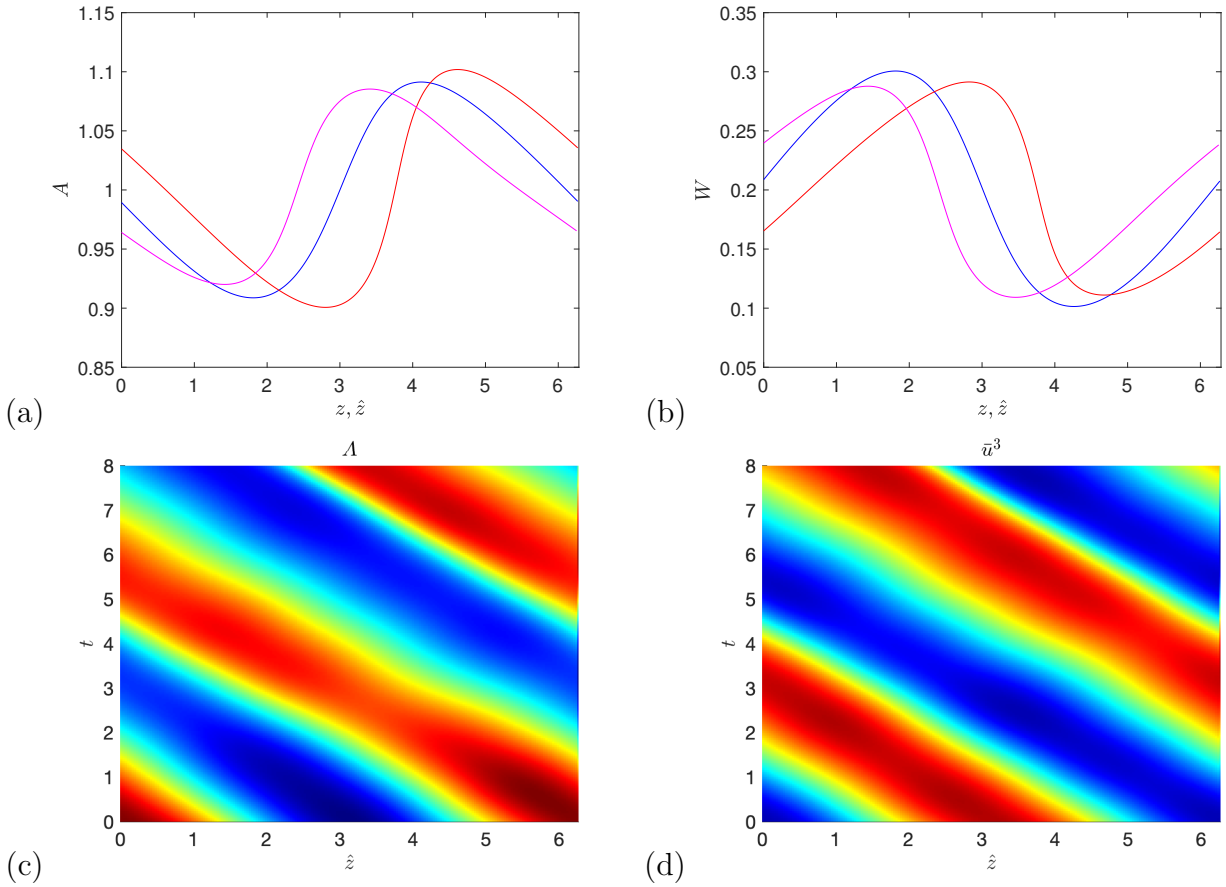

Fig. 10. Upstream wave. Profiles of (a) A and (b) W or $\bar{u}^3$ are plotted against $z \equiv \hat{z}$ at time $t = 8$, in the momentum wave model (blue), vorticity wave model (red) and slender vortex system (magenta). In (c,d) the evolution of A and $\bar{u}^3$ respectively are shown for the slender vortex model in the $(\hat{z}, t)$ plane.

disturbances. In the full slender vortex system, waves travelling downstream move faster than upstream, relative to the mean flow in the vortex, as is evident in figures 9, 10. This asymmetry is captured by the vortex wave model, but cannot be by the momentum wave model, for the reasons discussed below (6.25). Note that our initial condition for the slender vortex system, of a quadratic profile for the axial flow in (5.18), is closer to the set-up for the vorticity wave model than for the momentum wave model. In our full numerics, we have not tried to impose the axial slug flow that is the basis of the momentum wave model, as this would create a vortex sheet on the surface $r = a$, leading rapidly to instability.

7 External irrotational flow

One advantage of our framework is that it is relatively straightforward to include the effects of an external irrotational flow on the vortex. This enables us to study the effect of a uniform strain field, or of more complex external flows modelling the interactions of vortices. In the

physical variables $(\tilde{r}, \tilde{z})$ let the irrotational flow be given by

$$\tilde{\boldsymbol{U}}_{\rm ext} = \tilde{U}^1_{\rm ext}\,\partial_{\tilde{r}} + \tilde{U}^3_{\rm ext}\,\partial_{\tilde{z}} = U_{\rm ext}\,\hat{\boldsymbol{r}} + W_{\rm ext}\,\hat{\boldsymbol{z}}, \tag{7.1}$$

with $W_{\rm ext}$ depending on the axial coordinate and time, but not on radius $\tilde{r}$. We introduce the stream function $\psi_{\rm ext}$,

$$\psi_{\rm ext} = \tfrac{1}{2}\tilde{r}^2\,W_{\rm ext}, \tag{7.2}$$
$$U_{\rm ext} = -\tilde{r}^{-1}\,\partial_{\tilde{z}}\psi_{\rm ext} = -\tfrac{1}{2}\tilde{r}\,\partial_{\tilde{z}}W_{\rm ext}, \tag{7.3}$$
$$W_{\rm ext} = \tilde{r}^{-1}\,\partial_{\tilde{r}}\psi_{\rm ext}. \tag{7.4}$$

Since our vortex is slender, we may regard it as situated along the z-axis but subjected to this external flow. In the Lagrangian coordinates the (same) stream function $\boldsymbol{\psi}_{\rm ext} = \psi_{\rm ext}\,d\theta = \psi_{\rm ext}\,d\tilde{\theta}$, applies with $W_{\rm ext} = W_{\rm ext}(z,t)$ and

$$\psi_{\rm ext} = \tfrac{1}{2}F^2\,W_{\rm ext}, \tag{7.5}$$
$$u^1_{\rm ext} = -\tfrac{1}{2}FF_r^{-1}h'^{-1}W'_{\rm ext} - F_zF_r^{-1}h'^{-1}W_{\rm ext}, \tag{7.6}$$
$$u^3_{\rm ext} = h'^{-1}W_{\rm ext}, \tag{7.7}$$

making use of (4.22). Thus to specify an external axial flow along the vortex, we simply add these terms to the stream function and velocity components determined above in section 6.1. No contribution is made to the vorticity. We will consider this both in the context of the exact system for a slender vortex discussed in section 5, and for the vorticity wave model in section 6. We will not consider the momentum wave model further since our main interest here is vorticity dynamics and, as discussed in §2, in a uniform strain field only the vorticity wave model captures correctly the conservation of W/A and so faithfully represents the evolution of the vorticity field in this case.

7.1 Vorticity wave model with external flow

For the vorticity wave model of section 6 it is straightforward to include the external flow above by replacing

$$\psi \to \psi + \psi_{\rm ext} = \psi + \tfrac{1}{2}r^2f^2W_{\rm ext}, \tag{7.8}$$
$$u^1 \to u^1 + u^1_{\rm ext} = u^1 - \tfrac{1}{2}r(f^2W_{\rm ext})', \tag{7.9}$$
$$u^3 \to u^3 + u^3_{\rm ext} = u^3 + f^2W_{\rm ext}, \tag{7.10}$$

in (6.10), using $f^2h' = 1$. Then (6.11) becomes

$$U^3 = \dot{h}/h' = f^2\dot{h} = \bar{u}^3 = \tfrac{1}{4}\chi f^4a^2 + f^2W_{\rm ext}. \tag{7.11}$$

and if we set $W = \frac{1}{4}\chi f^2a^2$ as before we obtain the governing equations as

$$A\,\partial_t\left(\frac{W}{A}\right) = \frac{\Gamma^2}{8\pi J}\,\partial_z\left(\frac{1}{A}\right), \quad \partial_tJ = \partial_z(W + W_{\rm ext}), \quad AJ = \pi a^2. \tag{7.12}$$

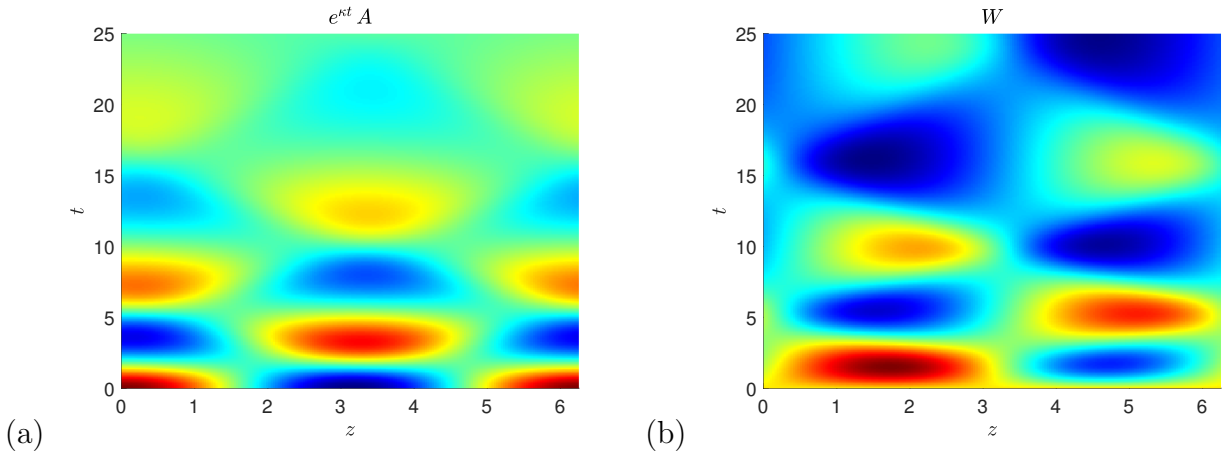

Fig. 11. Vorticity wave simulations for the initial $A(z,0)$ in (5.16), $W_0 = 0.1$ and uniform expansion with $\kappa = 0.1$: (a) $e^{\kappa t}A$ (from 0.9 to 1.1) and (b) W (from -0.05 to 0.18) are shown in the (z,t)-plane, z being the Lagrangian coordinate.

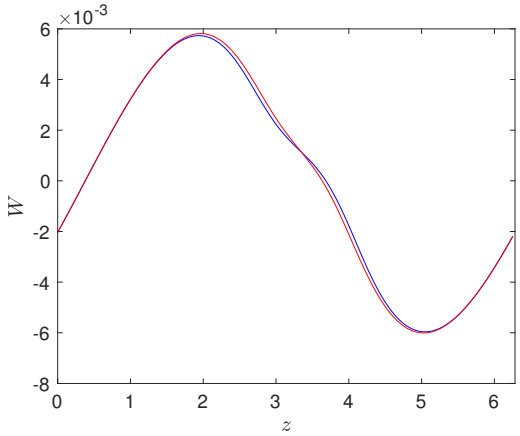

Fig. 12. For a continuation of the run in figure 11, W is plotted at time $t = 100$ (blue) together with the right-hand side of (7.17) (red).

The total axial flow is $W + W_{\text{ext}}$ but only the rotational part W contributes to the azimuthal vorticity as measured by W/A. The effect of W_{ext} is just to modify the evolution of the Jacobian J and area A in the Lagrangian coordinate system.

We consider the case of uniform expansion

$$W_{\text{ext}}(z,t) = \kappa\tilde{z} = \kappa h(z,t), \tag{7.13}$$

where $\kappa > 0$ is a constant, and use the non-dimensional system (6.20) with W replaced by $W + W_{\text{ext}}$. The equation for the Jacobian becomes

$$\partial_t J = \partial_z(W + \kappa h) = \partial_z W + \kappa J, \tag{7.14}$$

and the resulting equations may be written in conservation form as

$$(WJ, e^{-\kappa t}J): \quad \partial_t(WJ) = \partial_z(e^{\kappa t}(e^{-\kappa t}J)), \quad \partial_t(e^{-\kappa t}J) = \partial_z(e^{-2\kappa t}(WJ)/(e^{-\kappa t}J)). \tag{7.15}$$

Figure 11 shows a run in which a strain field with strength $\kappa = 0.1$ is superposed on the

earlier vorticity wave simulation depicted in figure 8. The waves can be seen to slow down and become less intense. For large times, the induced axial flow $W(z,t)$ tends to become subdominant to $W_{\rm ext}$ and so becomes decoupled from the dynamics and independent of time. By neglecting W in the equation for J and solving this to give

$$J(z,t) \simeq e^{\kappa t} J_\infty(z), \quad A(z,t) \simeq e^{-\kappa t} A_\infty(z), \quad t \to \infty, \tag{7.16}$$

we find that

$$W \simeq \frac{\Gamma^2}{8\pi^2 a^2 \kappa} \frac{J'_\infty}{J_\infty} = -\frac{\Gamma^2}{8\pi^2 a^2 \kappa} \frac{A'_\infty}{A_\infty}, \quad t \to \infty. \tag{7.17}$$

Thus the axial flow induced by the area waves becomes frozen out, subdominant to the exponentially increasing external stretching. This is evident in a longer run to $t = 100$ shown in figure 12. Note that in all these runs the Lagrangian coordinate z is used for plotting, whereas the corresponding range of physical space coordinate $\tilde{z}$ is increasing exponentially as $2\pi e^{\kappa t}$.

7.2 Slender vortex dynamics with external flow

We now consider the full slender vortex model under the influence of an imposed, irrotational external flow given by $\psi_{\rm ext}$ in (7.5). In our earlier simulations of the slender vortex system we set $h' = 1$, $\dot{h} = 0$, $\tilde{z} = z$. When there is an external irrotational flow present, it is sensible to choose h to absorb it into the coordinate system. All that will be left are some factors in the equations which represent the geometrical effect of stretching in the coupling of various quantities.

Again it is helpful to first suppose there is no vortex present. Then $\zeta_3 = 0$ and we have only irrotational flow. We absorb this into the *background coordinate system motion* by setting

$$U^1_{\rm ext} = u^1_{\rm ext}, \quad U^3_{\rm ext} = u^3_{\rm ext}, \tag{7.18}$$

and defining $F_{\rm ext} = r f_{\rm ext}(z,t)$ and $h_{\rm ext}(z,t)$, by integrating

$$\dot{f}_{\rm ext} = -\tfrac{1}{2} f_{\rm ext} \frac{W'_{\rm ext}}{h'_{\rm ext}}, \quad \dot{h}_{\rm ext} = W_{\rm ext}, \tag{7.19}$$

with respect to time. With these definitions, equations (4.25, 4.27) are satisfied, with $v^3 = 0$ and all quantities labelled by 'ext'. We can also impose

$$f^2_{\rm ext} h'_{\rm ext} = 1 \tag{7.20}$$

at time $t = 0$ and then this condition is preserved subsequently. All we have done is ensure that a point labelled by constant (r,z) is a Lagrangian parcel in the external flow.

In the presence now of vorticity, we choose to keep the same evolution of h, setting $h = h_{\rm ext}$, but allow additional flexing in radius F so that the coordinate system continues to follow vorticity surfaces in real space. In this more general situation, we retain the above definitions

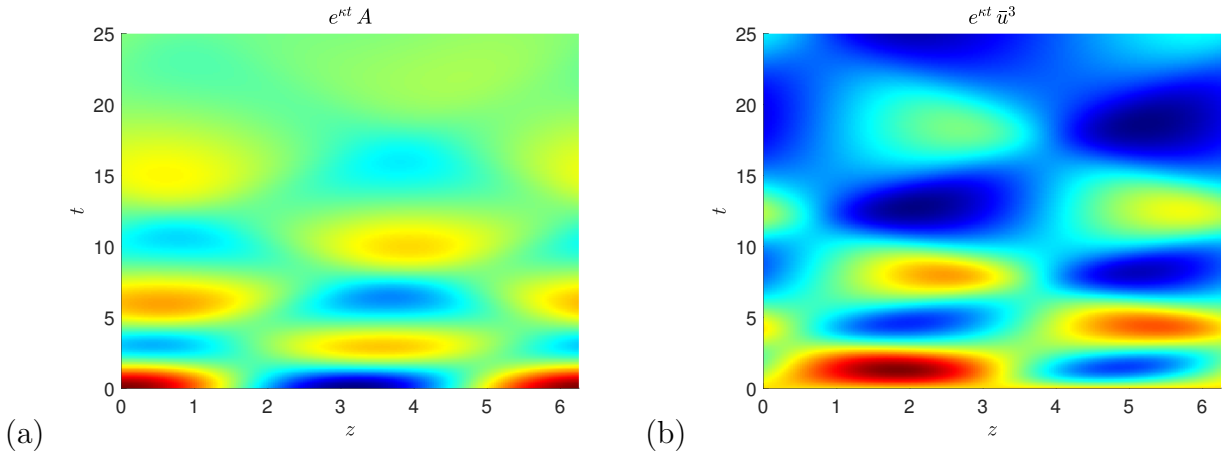

Fig. 13. Slender vortex simulations for the initial $A(z,0)$ in (5.16), $W = 0.1$ and uniform expansion with $\kappa = 0.1$: (a) $e^{\kappa t}A$ (from 0.9π to 1.1π) and (b) $e^{\kappa t}\,\bar{u}^3$ (from -0.035 to 0.172) are shown in the (z,t)-plane, z being the Lagrangian coordinate.

of $\psi_{\rm ext}$, $U^1_{\rm ext}$, $U^3_{\rm ext}$, $h_{\rm ext}$, $f_{\rm ext}$ and make the following replacements,

$$\psi \to \psi + \psi_{\rm ext}, \quad h \to h_{\rm ext}, \quad F \to F f_{\rm ext}, \tag{7.21}$$

$$u^1 \to u^1_{\rm ext} + u^1, \quad u^3 \to u^3_{\rm ext} + u^3, \quad U^1 \to U^1_{\rm ext} + U^1, \quad U^3 \to U^3_{\rm ext}, \tag{7.22}$$

in the governing equations, (4.15, 4.22, 4.24–4.27, 5.6), to give

$$\partial_t \zeta_2 + (v^3\zeta_2)_z = \zeta_3 \partial_z v^2, \tag{7.23}$$

$$\zeta_2 = -(h'_{\rm ext})^2\,[(FF_r)^{-1}\psi_r]_r, \tag{7.24}$$

$$u^1 = U^1 = -(FF_r)^{-1}\,\psi_z = F_r^{-1}\dot{F}, \tag{7.25}$$

$$u^2 = v^2 = F^{-2}h'_{\rm ext}\,\nu_2, \tag{7.26}$$

$$u^3 = v^3 = (FF_r)^{-1}\,\psi_r. \tag{7.27}$$

Thus, all other things being equal, stretching when $h'_{\rm ext} > 0$ reduces the flow generated for a given azimuthal vorticity ζ_2 distribution, but intensifies the azimuthal v^2 component, through angular momentum conservation.

We again undertake a simulation for pure exponential stretching with, for constant κ,

$$h_{\rm ext} = ze^{\kappa t}, \quad f_{\rm ext} = e^{-\frac{1}{2}\kappa t}, \quad W_{\rm ext} = \kappa z e^{\kappa t}. \tag{7.28}$$

Figure 13 shows a simulation and we again see the area waves petering out as t increases. Note that by virtue of (4.7) the earlier W in figure 11 should be compared with $\bar{u}^3\partial_z = h'\bar{u}^3\partial_{\tilde{z}} = e^{\kappa t}\bar{u}^3\hat{\boldsymbol{z}}$ here. The comparison with figure 11 for the vorticity model is good, noting that the two horizontal coordinates z are not quite the same (in the earlier simulation this includes the motion with the background flow $W + W_{\rm ext}$ whereas for the present one it includes only $W_{\rm ext}$).

To analyse the limit as $t \to \infty$, given $\kappa > 0$ note that the following orders of magnitude hold,

$$\zeta_3, \nu_2, F = O(1), \quad \zeta_2, v^2 = O(e^{\kappa t}), \quad \psi, u^1, U^1, u^3, v^3, \dot{F} = O(e^{-\kappa t}), \tag{7.29}$$

and so evolution of the vortex profile, given by F, freezes out. In (7.23) the $(v^3\zeta_2)_z$ term becomes negligible as $t \to \infty$. Given that F becomes time-independent, $\zeta_3 = \zeta_3(r)$ and $\nu_2 = \nu_2(r)$, this

equation may be integrated to leave

$$\zeta_2 = \kappa^{-1} e^{\kappa t} \zeta_3 \nu_2 \, \partial_z F^{-2}. \tag{7.30}$$

Thus the azimuthal vorticity profile ζ_2 becomes linked to the vortex shape and ζ_2 grows exponentially as $e^{\kappa t}$. The corresponding axial flow component $u^3 = O(e^{-\kappa t})$ but as mentioned above this needs multiplying by $e^{\kappa t}$ when referred to the usual unit vector $\hat{\boldsymbol{z}}$; in short the actual measured axial flow $e^{\kappa t} u^3$ again becomes frozen in time at $O(1)$ levels, as for the vorticity wave model (figure 12 and (7.17)).

8 Singular external flows

Following LA89 it is clear that if an external irrotational disturbance compresses a vortex locally, area waves rush in to restore the cross sectional area. However we have seen that the effect of uniform axial stretching is to freeze the evolution of area waves, so that the resulting vortex profile is simply passively stretched in the external flow. This then raises the question of the competition between these two effects: if an external stretching flow itself introduces a small and shrinking scale into the evolution, when do area waves act to restore the cross section, and when are they defeated by freezing?

We explore this briefly in the context of the vorticity wave model, working from the governing equations (7.12), and looking principally at scaling properties. We consider a similarity form of $W_{\rm ext}$ in which the spatial scale collapses to zero at a time t_* while the velocities increase. Although this is a somewhat artificial problem in the context of waves on a columnar vortex, the goal is to throw light on more complex problems such as the collision of vortex filaments, something we return to in our concluding discussion.

We let $\tau = t_* - t$ and so $\partial_t = -\partial_\tau$. We assume the axial flow is given by a Lagrangian map of the form

$$h_{\rm ext}(z,t) = \tau^\beta \, \hat{h}_{\rm ext}(\xi), \quad \xi = z/\tau^\alpha. \tag{8.1}$$

Suppose first there is no vortex present so that we have $W_{\rm ext} = \dot{h}_{\rm ext}$, $J = h'_{\rm ext}$, with

$$W_{\rm ext} = \dot{h}_{\rm ext} = \tau^{\beta-1} \, \hat{W}_{\rm ext}(\xi), \quad J = h'_{\rm ext} = \tau^{\beta-\alpha} \, \hat{J}(\xi), \quad A = \tau^{\alpha-\beta} \, \hat{A}(\xi), \tag{8.2}$$

and so

$$\hat{W}_{\rm ext} = -\beta \hat{h}_{\rm ext} + \alpha \xi \hat{h}'_{\rm ext}, \quad \hat{J} = \hat{h}'_{\rm ext}, \quad \hat{A}\hat{J} = \pi a^2. \tag{8.3}$$

We now introduce a vortex, and axial variations in area will tend to drive area waves given by W: we can use the first of (7.12) to estimate the scaling of W as

$$W = \tau^{1-\alpha} \, \hat{W}(\xi), \tag{8.4}$$

with this equation becoming

$$(2\alpha - \beta - 1)\hat{A}\hat{W} + \alpha\xi(\hat{A}\hat{W}' - \hat{A}'\hat{W}) = -\frac{\Gamma^2}{8\pi^2 a^2} \, \hat{A}'. \tag{8.5}$$

Comparing (8.2, 8.4), the condition that the driven axial flow W is comparable with the external flow $W_{\rm ext}$ is

$$\alpha + \beta = 2. \tag{8.6}$$

If $\alpha + \beta > 2$ then $W_{\rm ext}$ is dominant and area waves die out as $\tau \to 0$. However if $\alpha + \beta < 2$ then W will tend to dominate and the area waves will rush in to keep the vortex cross section from becoming singular in the limit. The critical, transitional case is $\alpha + \beta = 2$ where neither flow can be ignored; in a future study we will examine similarity solutions that solve (8.5), and their properties.

To connect this with other studies, note that while for Lagrangian coordinates,

$$\partial_z \sim \tau^{-\alpha}, \quad \partial_t \sim \tau^{-1}, \tag{8.7}$$

for Eulerian coordinates we have

$$\partial_{\tilde z} \sim \tau^{-\beta}, \quad \partial_{\tilde t} \sim \tau^{-1}. \tag{8.8}$$

Since $\tilde z/\tau^\beta = \hat h_{\rm ext}(z/\tau^\alpha)$ we see the symmetry between the treatment of the two spatial coordinates as expressed above. Leray (1934) scalings are often used in studies of vortex stretching and potential singularity formation and here correspond to $\alpha = 3/2$ and $\beta = 1/2$, so that the axial $\tilde z$ scale and vortex radius $A^{1/2}$ decrease as $\tau^{1/2}$ while the velocity $W_{\rm ext}$ increases as $\tau^{-1/2}$. This satisfies condition (8.6) and indicates that in a slender vortex configuration involving Leray scalings, area wave dynamics should be considered in analysing the vortex evolution. This could be done by developing an asymptotically correct slender vortex system, or through averaging to yield a model akin to the vorticity wave model of L94 which, as discussed in the present paper, has the scope to capture key effects of area waves in potentially frustrating local vortex collapse and singularity formation.

9 Discussion

In this paper we have given a discussion of area waves on a columnar vortex using a Lagrangian framework, strictly a hybrid Eulerian–Lagrangian framework, with a focus on the limit of a long-wave disturbances, in other words the slender vortex limit. Our approach involves tracking the vorticity distribution via a map from the Lagrangian to the physical space, which preserves the vorticity and enables a detailed comparison between the slender vortex dynamics and the models of LA89 and L94, both analytically and numerically. Note that although it is straightforward to write down the exact equations in generality without taking the slender vortex limit, the difficulty of inverting the vorticity distribution to find the corresponding fluid flow means that it is unlikely to be a useful way of understanding phenomena such as vortex breakdown, when shock-like behaviour breaks any imposed separation of scales. However in the slender limit the equations become tractable to numerics and further approximations. We have given simulations of the full slender vortex equations and compared them with the momentum wave model of LA89 and the vorticity wave model of L94. Both models show a good comparison with the full slender system, giving travelling and standing waves with the correct structure and reasonable agreement with the velocities involved. When there is a mean axial flow, the full system has an asymmetry between waves propagating upstream and those

propagating downstream, which can understood in terms of the vorticity distribution. As a result, this effect is best captured by the vorticity wave model; the momentum wave model has an extra symmetry that equates upstream and downstream waves. We should also qualify our comparisons by noting that the initial conditions we use in our simulations are closer to the model flows in the vorticity wave model than those in the momentum wave model (which would involve vortex sheets). In the present paper we have also restricted to waves on a straight vortex, and we plan to extend the Euler–Lagange approach to more complex centreline geometry. This would allow us to assess the various area wave models against the full core dynamics and so make contact with studies of the effects of axial flow on vortex ring motion and instabilities (e.g. Lundgren & Ashurst, 1989; Margerit & Brancher, 2001; Margerit, 2002; Ting, Klein & Knio, 2007). We have also not considered the stability properties of the vortices we have used, with constant axial vorticity and quadratic axial flow; the case of zero axial flow $W = 0$ is well known to be stable (see, e.g., Saffman, 1992). Studies of more general profiles, in particular the smooth Batchelor vortex, indicate stability provided the axial flow is not too strong (see, e.g. Lessen, Singh & Paillet, 1974).

The approach based on differential geometry, that is the explicit use of metric and volume forms, has many advantages, one in particular being that it gives convenient bases for writing down the velocity, the momentum and the vorticity in any context. The separation between the velocity as an advecting vector field, and the momentum as a 1-form field, is crucial and once this is made, the Euler and vorticity equations have an intuitive form. Another advantage is the complete flexibility in coordinates; however there is a corresponding disadvantage, that the physical components of the flow and vorticity field, referred to a standard orthogonal coordinate system, are not as accessible. The Lagrangian systems we develop allow an external straining flow to be incorporated with little difficulty. Simulations of the slender vortex system and the vorticity wave model both show area waves freezing and the vortex profile becoming passive under uniform axial strain.

We have also investigated similarity scalings where an external irrotational flow involves increasing axial velocities over a shrinking scale. Although this is a somewhat artificial problem in the present context of an axisymmetric columnar vortex, we pursued it because analogous processes operate when vortices collide and stretch each other in three dimensions. Here we find that depending on the exponents governing the external flow, area waves may dominate and tend to impose a uniform vortex cross section, or stretching may dominate and tend to freeze out the area waves. The transitional case where both phenomena are present — neither may *a priori* be ignored — includes the Leray (1934) scalings used in many singularity studies; for example see Pumir & Siggia (1987), Pelz (2001), Moffatt & Kimura (2019a) and references therein. Of course we have only looked at this in the most straightforward, axisymmetric context, and real problems involving colliding vortices are highly three-dimensional. Nonetheless if we apply the Leray scalings to our system, admittedly a somewhat artifical step, we can conclude that it may be perilous to ignore axial flow in other idealised models of vortex stretching and potential singularity formation; the area wave restoring mechanism may draw fluid in to prevent the local thinning of a vortex.

Another phenomenon which may well be important is that colliding vortices will generally change cross sectional shape, not only the obvious distortion from circle to ellipse, but through an inevitable *erosion* of vorticity as induced flows drive vortices together (Pumir & Siggia,

1987; Hormoz & Brenner, 2012; Childress, Gilbert & Valiant, 2016). This has the general effect of making the circulation of colliding vortex cores a function of the axial component and time, impacting on similarity scalings (Childress & Gilbert, 2018). With the tools developed in the present paper, we plan further studies with an eye towards more three-dimensional configurations where vortices may pair and stretch intensely; see, for example, Takaki & Hussain (1984), Pumir & Siggia (1987), Saffman (1990), Klein, Majda & Damodaran (1995), Bustamante & Kerr (2008) and Moffatt & Kimura (2019a,b).

A Some equations in terms of components

In this appendix we note some of the formulae from the early part of section 3.1 in coordinate form, as this may be more familiar to some readers; we drop the tildes for convenience. The Euler and related equations (3.1–3.3) evolve the momentum $\boldsymbol{\nu}$ in the flow field $\boldsymbol{u}$ with pressure p acording to

$$\partial_t \nu_i + u^j \partial_j \nu_i + \nu_j \partial_i u^j + \partial_i (p - \tfrac{1}{2} u^j \nu_j) = 0, \tag{A.1}$$

$$\nu_i = g_{ij} u^j, \tag{A.2}$$

$$\partial_i (\mu u^i) = 0. \tag{A.3}$$

The metric $\boldsymbol{g}$ links momentum and velocity in (A.2), and the square root of its determinant, $\mu = |\boldsymbol{g}|^{1/2}$, comes into the incompressibility condition (A.3). For vorticity, we have defined the vorticity 2-form $\boldsymbol{\zeta} = d\boldsymbol{\nu}$, which can be thought of as the anti-symmetric 2-tensor with

$$\boldsymbol{\zeta} = \zeta_{ij}\, dx^i \otimes dx^j = \tfrac{1}{2} \zeta_{ij}\, dx^i \wedge dx^j, \tag{A.4}$$

defined by (3.5),

$$\zeta_{ij} = \partial_i \nu_j - \partial_j \nu_i, \tag{A.5}$$

and which evolves according to (3.4), which is

$$\partial_t \zeta_{ij} + u^k \partial_k \zeta_{ij} + \zeta_{kj} \partial_i u^k + \zeta_{ik} \partial_j u^k = 0. \tag{A.6}$$

To pick on one component, say ζ_{12}, we have

$$\partial_t \zeta_{12} + u^k \partial_k \zeta_{12} + \zeta_{12} \partial_1 u^1 + \zeta_{32} \partial_1 u^3 + \zeta_{12} \partial_2 u^2 + \zeta_{13} \partial_2 u^3 = 0. \tag{A.7}$$

As we are undertaking explicit calculations we find it convenient to set, cf. (3.30),

$$\zeta_1 = \zeta_{23} = -\zeta_{32}, \quad \zeta_2 = \zeta_{31} = -\zeta_{13}, \quad \zeta_3 = \zeta_{12} = -\zeta_{21}, \tag{A.8}$$

and so, adding and subtracting a term of $\zeta_3 \partial_3 u^3$, we obtain

$$\partial_t \zeta_3 + (u^1\partial_1 + u^2\partial_2 + u^3\partial_3)\zeta_3 - (\zeta_1\partial_1 + \zeta_2\partial_2 + \zeta_3\partial_3)u^3 + (\partial_1 u^1 + \partial_2 u^2 + \partial_3 u^3)\zeta_3 = 0, \tag{A.9}$$

which is essentially the version which emerges in (3.35), and similarly for ζ_1 and ζ_2.

Instead of the vorticity considered as the 2-form field $\boldsymbol{\zeta}$, we can think of it as a vector field $\boldsymbol{\omega}$, with $\boldsymbol{\omega} \lrcorner \boldsymbol{\mu} = \boldsymbol{\zeta}$ or

$$\zeta_{ij} = \mu \varepsilon_{ijk} \omega^k, \quad \omega^i = \tfrac{1}{2} \mu^{-1} \varepsilon^{ijk} \zeta_{jk} \tag{A.10}$$

or even,

$$\omega^1 = \mu^{-1}\zeta_1, \quad \omega^2 = \mu^{-1}\zeta_2, \quad \omega^3 = \mu^{-1}\zeta_3. \tag{A.11}$$

This vector field is Lie-dragged also in incompressible flow,

$$\partial_t \boldsymbol{\omega} + \mathcal{L}_{\boldsymbol{u}}\, \boldsymbol{\omega} = 0, \tag{A.12}$$

or in components

$$\partial_t\, \omega^i + u^j\, \partial_j \omega^i - \omega^j\, \partial_j u^i = 0. \tag{A.13}$$

We could work with $\boldsymbol{\zeta}$ or $\boldsymbol{\omega}$ in our study but have preferred to use $\boldsymbol{\zeta}$ as it is more simply related to the momentum $\boldsymbol{\nu}$ via (A.5) and thence to the velocity field via (A.2): only the metric components g_{ij} (and not the volume element μ) then appear in the elliptic problem going from the vorticity 2-form field $\boldsymbol{\zeta}$ to the flow field $\boldsymbol{u}$.

B The Lundgren–Ashurst model system

We present a derivation of the LA89 model for momentum-based area waves within our framework, by averaging the Euler equation rather than the vorticity equation. The Euler equation is written in generality in (3.26–3.29). We set $\partial_\theta = 0$, $U^2 = 0$, and under the slender vortex scalings (5.2–5.4) obtain at leading order,

$$-v^2\nu_{2r} - v^3\nu_{3r} + \tfrac{1}{2}(v^2\nu_2 + v^3\nu_3 - U^3\nu_3)_r + p_r = 0, \tag{B.1}$$

$$(\partial_t + v^1\partial_r + v^3\partial_z)\nu_2 = 0, \tag{B.2}$$

$$(\partial_t + v^1\partial_r + v^3\partial_z)\nu_3 - v^2\nu_{2z} - v^3\nu_{3z} + \tfrac{1}{2}(v^2\nu_2 + v^3\nu_3 - U^3\nu_3)_z + p_z = 0. \tag{B.3}$$

Now we need to relate velocity and momentum, and jump straight to using the simplified metric with $F = rf(z,t)$ and $f^2h' = 1$. Equations (4.22–4.27) give

$$u^1 = U^1 + v^1 = -r^{-1}\psi_z, \quad u^2 = v^2, \quad u^3 = U^3 + v^3 = r^{-1}\psi_r, \tag{B.4}$$

$$\nu_1 = f^2u^1 + rff'u^3, \quad \nu_2 = r^2f^2v^2, \quad \nu_3 = f^{-4}u^3. \tag{B.5}$$

Next we use $U^3 = U^3(z,t)$, $f = f(z,t)$, and the relationship between ν_2, ν_3 and u^2, u^3 above to simplify (B.1, B.3) as

$$-r^{-3}f^{-2}(\nu_2)^2 + p_r = 0, \tag{B.6}$$

$$(\partial_t + v^1\partial_r + v^3\partial_z)\nu_3 + \tfrac{1}{2}(v_z^2\nu_2 - v^2\nu_{2z}) + \tfrac{1}{2}(v_z^3\nu_3 - v^3\nu_{3z}) - \tfrac{1}{2}(U^3\nu_3)_z + p_z = 0. \tag{B.7}$$

We gain the leading order centrifugal pressure balance in the radial equation, and in the axial equation we have grouped the terms in a useful fashion. So far everything is exact in the slender vortex limit with the chosen metric. To make further progress we need to make some assumptions of a modelling nature. We take u^1 to be proportional to r so that the radial motion is absorbed into the evolution of the coordinate system giving $v^1 = 0$, $u^1 = U^1$. This corresponds to applying our first modelling assumption from section 6 that the radial flow is a uniform contraction or expansion. We take the axial flow again to be a slug flow, as per our second assumption and set $v^3 = 0$, $u^3 = U^3$. The evolution equations (B.2, B.7) for ν_2 and ν_3

become, after some simplification,

$$\partial_t \nu_2 = 0, \tag{B.8}$$
$$f^{-2}\partial_t^2 h = -\tfrac{1}{2} r^{-2} (f^{-2})' \nu_2^2 - p_z. \tag{B.9}$$

In obtaining (B.9) we have used (B.8) and chosen some profile for $\nu_2(r)$ independent of z. We have also used freely that $f^2 h' = 1$ and so $f^4 \nu_3 = u^3 = U^3 = \dot{h}/h' = f^2 \dot{h}$.

Equation (B.6) gives the pressure; from integrating and requiring continuity at $r = a$ and tending to zero at infinity, we obtain

$$p = \begin{cases} \tfrac{1}{2}\Omega^2 (r^2 - 2a^2) f^{-2}, & r \le a, \\ -\tfrac{1}{2}\Omega^2 a^4 r^{-2} f^{-2}, & r > a. \end{cases} \tag{B.10}$$

With this, minus the right-hand side of (B.9) simplifies to

$$p_z + \tfrac{1}{2} r^{-2} (f^{-2})' (\nu_2)^2 = \Omega^2 (r^2 - a^2)(f^{-2})', \qquad r \le a, \tag{B.11}$$

and zero for $r > a$. In the axial momentum equation (B.9), the left-hand side depends only on (z, t) while the right-hand side has radial dependence. The assumption of driving a slug flow is not warranted by the exact dynamics. Thus we average the right-hand side of (B.11) over $0 \le r \le a$ and gain the model axial momentum equation as

$$f^{-2}\partial_t^2 h = \tfrac{1}{2}\Omega^2 a^2 (f^{-2})'. \tag{B.12}$$

We now set $\dot{h} = W$, $\Gamma = 2\pi\Omega a^2$, $A = \pi a^2 f^2$ and $J = h' = f^{-2}$ to obtain

$$\partial_t W = \frac{\Gamma^2}{8\pi J}\, \partial_z \left(\frac{1}{A} \right), \tag{B.13}$$

which is the LA89 area wave model as required.

Acknowledgements

The authors are very grateful to the Leverhulme Trust, which supported ADG and this collaboration through the award of a Research Fellowship. ADG also acknowledges support by the EPSRC under grant EP/T023139/1. We thank Jacques Vanneste for numerous discussions on matters of fluid flow and differential geometry. We appreciate the helpful critique and useful references to the literature from the referees.

References

Abid, M., Andreotti, B., Douady, S. & Nore, C. 2002 Oscillating structures in a stretched–compressed vortex. *J. Fluid Mech.* **450**, 207–233.

Arnold, V.I. & Khesin, B.A. 1998 *Topological methods in hydrodynamics*. Springer–Verlag, Applied Mathematical Sciences, vol. 125.

Besse, N. & Frisch, U. 2017 Geometric formulation of the Cauchy invariants for incompressible Euler flow in flat and curved spaces. *J. Fluid Mech.* **825**, 412–478.

Bühler, O. 2014 *Waves and mean flows*, 2nd edition. Cambridge University Press.

Bustamante, M.D. & Kerr, R.M. 2008 3D Euler about a 2D symmetry plane. *Physica D* **237**, 1912–1920.

Callegari, A.J. & Ting, L. 1978 Motion of a curved vortex filament with decaying vortical core and axial velocity. *SIAM J. Appl. Math.* **35**, 148–175.

Childress, S., Gilbert, A.D. & Valiant, P. 2016 Eroding dipoles and vorticity growth for Euler flows in $\mathbb{R}^3$: axisymmetric flow without swirl. *J. Fluid Mech.* **805**, 1–30.

Childress, S. & Gilbert, A.D. 2018 Eroding dipoles and vorticity growth for Euler flows in $\mathbb{R}^3$: the hairpin geometry as a model for finite-time blowup. *Fluid Dyn. Res.* **50**, article 011418.

Frankel, T. 1997 *The geometry of physics*. Cambridge University Press.

Fukumoto, Y. & Miyazaki, T. 1991 Three-dimensional distortions of a vortex filament with axial velocity. *J. Fluid Mech.* **222**, 369–416.

Gilbert, A.D. & Vanneste, J. 2018 Geometric generalised Lagrangian-mean theories. *J. Fluid Mech.* **839**, 95–134.

Hawking, S.W. & Ellis, G.F.R. 1973 *The large scale structure of space-time*. Cambridge University Press.

Hormoz, S. & Brenner, M.P. 2012 Absence of singular stretching of interacting vortex filaments. *J. Fluid Mech.* **707**, 191–204.

Klein, R. & Ting, L. 1992 Vortex filament with axial core structure variation. *Appl. Math. Lett.* **5**, 99–103.

Klein, R. & Majda, A.J. 1991a Self-stretching of a perturbed vortex filament. I. The asymptotic equation for deviations from a straight line. *Physica D* **49**, 323–352.

Klein, R. & Majda, A.J. 1991b Self-stretching of a perturbed vortex filament. II. Structure of solutions. *Physica D* **53**, 267–294.

Klein, R., Majda, A.J. & Damodaran, K. 1995 Simplified equations for the interaction of nearly parallel vortex filaments. *J. Fluid Mech.* **288**, 201–248.

Leibovich, S. 1978 The structure of vortex breakdown. *Ann. Rev. Fluid Mech.* **10**, 221–246.

Leonard, A. 1994 Nonlocal theory of area-varying waves on axisymmetric vortex tubes. *Phys. Fluids* **6**, 765–777, referred to as L94 in the text.

Leray, J. 1934 Sur un liquide visqueux emplissant l'espace. *Acta Math.* **63**, 193–248.

Lessen, M., Singh, P.J. & Paillet, F. 1974 The stability of a trailing line vortex. Part I. Inviscid theory. *J. Fluid Mech.* **63**, 753–763.

Lundgren, T.S. & Ashurst, W.T. 1989 Area-varying waves on curved vortex tubes with application to vortex breakdown. *J. Fluid Mech.* **200**, 283–307, referred to as LA89 in the text.

Margerit, D. 2002 Axial core-variations of axisymmetric shape on a curved slender vortex filament with a similar, Rankine, or bubble core. *Phys. Fluids* **14**, 4406–4428.

Margerit, D. & Brancher, J.-P. 2001 Asymptotic expansions of the Biot–Savart law for a slender vortex with core variation. *J. Eng. Math.* **40**, 297–313.

Marshall, J.S. 1991 A general theory of curved vortices with circular cross-section and variable core area. *J. Fluid Mech.* **229**, 311–338.

Marshall, J.S. 1992 Buckling of a columnar vortex. *Phys. Fluids A* **4**, 2620–2627.

Marshall, J.S. 1993 The effect of axial pressure gradient on axisymmetrical and helical vortex waves. *Phys. Fluids A* **5**, 588–599.

Melander, M.V. & Hussain, F. 1994 Core dynamics on a vortex column. *Fluid Dynam. Res.*

13, 1–37.

Moffatt, H.K. & Kimura, Y. 2019a Towards a finite-time singularity of the Navier–Stokes equations. Part 1. Derivation and analysis of dynamical system. *J. Fluid Mech.* **861**, 930–967.

Moffatt, H.K. & Kimura, Y. 2019b Towards a finite-time singularity of the Navier–Stokes equations. Part 2. Vortex reconnection and singularity evasion. *J. Fluid Mech.* **870**, R1.

Moore, D.W. & Saffman, P.G. 1972 The motion of a vortex filament with axial flow. *Phil. Trans. R. Soc. Lond. A* **272**, 403–429.

Nolan, D.S. 2001 The stabilizing effects of axial stretching on turbulent vortex dynamics. *Phys. Fluids* **13**, 1724–1738.

Pelz, R.B. 2001 Symmetry and the hydrodynamic blow-up problem. *J. Fluid Mech.* **444**, 299–320.

Pumir, A. & Siggia, E.D. 1987 Vortex dynamics and the existence of solutions to the Navier–Stokes equations. *Phys. Fluids* **30**, 1060–1626.

Saffman, P.G. 1990 A model of vortex reconnection. *J. Fluid Mech.* **212**, 395–402.

Saffman, P.G. 1992 *Vortex dynamics.* Cambridge University Press.

Schutz, B. 1980 *Geometrical methods of mathematical physics.* Cambridge University Press.

Soward, A.M. & Roberts, P.H. 2010 The hybrid Euler–Lagrange procedure using an extension of Moffatt's method. *J. Fluid Mech.* **661**, 45–72.

Takaki, R. & Hussain, A.K.M.F. 1984 Dynamics of entangled vortex filaments. *Phys. Fluids* **27**, 761–763.

Ting, L. 1971 Studies in the motion and decay of vortices. In *Aircraft wake turbulence and its detection* (ed. J.H. Olsen, A. Goldburg, M. Rogers), Plenum Press, New York.

Ting, L, Klein, R. & Knio, O.M. 2007 *Vortex dominated flows: analysis and cvomputation for multiple scale phenomena.* Applied Mathematical Sciences series, vol. **161**. Springer.

Tung, C. & Ting, L. 1967 Motion and decay of a vortex ring. *Phys. Fluids* **10**, 901–910.

Webb, G. 2018 *Magnetohydrodynamics and fluid dynamics: action principles and conservation laws.* Lecture Notes in Physics, vol. **946**. Springer.

Widnall, S.E. & Bliss, D.B. 1971 Slender body analysis of the motion and stability of a vortex filament containing an axial flow. *J. Fluid Mech.* **50**, 335–353.

Widnall, S.E., Bliss, D.B. & Zalay, A. 1971 Theoretical and experimental study of the stability of a vortex pair. In *Aircraft wake turbulence and its detection* (ed. J.H. Olsen, A. Goldburg, M. Rogers), Plenum Press, New York.